EXPERIMENTS ON THE RELATIONSHIP BETWEEN THE COEFFICIENTS OF FRICTION AND HEAT TRANSFER IN NUCLEATE BOILING

Thesis by

Hampton Emanuel Mulligan

Lieutenant Commander

United States Navy

In Partial Fulfillment of the Requirements

for the Degree of

Aeronautical Engineer

California Institute of Technology

Pasadena, California

1954

ACKNOWLEDGEMENT

The author wishes to express his appreciation of the helpful aid, criticism and encouragement from Professor R. H. Sabersky during the pursuit of this research. The author is indebted to Mr. N. Van De Verg of the Heat Transfer Section of the Jet Propulsion Laboratory and his staff--in particular, Mr. K. S. MacDavid for aid in setting up the experimental equipment, and Mr. D. R. Bartz and Mr. M. B. Noel for their general aid and advice. The author wishes to thank the personnel of the Central Recording Section for their cooperation during the tests, his patient wife for her typing of the manuscript and Mrs. Ruth Toy for her help in preparing the figures.

ABSTRACT

An experimental investigation was conducted to determine whether any relationship exists between the friction and the heat transfer coefficients in the region of nucleate boiling with forced convection. The tests were carried out with distilled water flowing through a 3/8 inch diameter tube. The water was heated by passing an electric current through the tube wall.

Measurements of the velocity of the water were taken at three positions along the test section by means of pitot tubes. The pitot tubes were also used to measure static pressure drops. From the experimental data the heat transfer and friction coefficients were computed. These coefficients were determined for a heat transfer range from 1.0 to 2.0 Btu/sq in-sec and for three pressure levels, 265, 115 and 65 psia.

It was found that for a constant subcooling in the nucleate boiling region the friction coefficient increases with increasing heat transfer rate, indicating that the bubbles actually do influence the momentum exchange. It was also found that the experimentally determined values of the friction and heat transfer coefficients plot about a line the equation of which is $\frac{C_F}{2} = C_H$. This is the relation that one would expect on the basis of Reynolds' analogy for turbulent flow either without a laminar boundary layer, or with the laminar boundary layer when the Prandtl number is unity. It appears therefore that the effect of the bubbles is a hydrodynamic one leading to an increase in heat exchange as well as in momentum exchange.

TABLE OF CONTENTS

TABLE OF CONTENTS (Cont'd)

I. INTRODUCTION

Boiling heat transfer is defined as heat transfer from a surface to a liquid when the temperature of the liquid adjacent to the surface is sufficiently high to cause vapor formation. The temperature of the bulk of the liquid may be either equal to or below the saturation temperature. The difference between the saturation temperature and the bulk temperature is called "subcooling".

Fig. 1 is a graph typical of the results found for boiling heat transfer under the conditions of either forced or free convection, with or without subcooling (1). The graph is plotted to show the relation of the heat transfer rate (Btu/sq in-sec) to the temperature of the heating surface. In the range from A to B heat is transferred by convection without boiling. When the surface temperature reaches a certain value somewhat above the boiling point of the liquid, the heat transfer rate increases sharply with increasing surface temperature until a maximum is reached at point C. Beyond point C the heat transfer rate decreases with increasing surface temperature. It then passes through a minimum at point D, and again increases with further increase of surface temperature.

The region from A to B is usually called the convection region; the region from B to C, the nucleate boiling region; from C to D, the partial film boiling region; and beyond D, the complete film boiling region.

At or near point B bubbles of vapor begin to form on the

surface. When the liquid is subcooled, the bubbles will grow to a certain size and then collapse again on the surface (1). The maximum size is greatly influenced by the amount of subcooling, the larger bubbles occurring at the lower subcooling (1, 2). With increase of surface temperature in the nucleate boiling region the population of the bubbles increases. Beyond point C the bubble population becomes so great that the bubbles begin to coalesce and to form fairly large vapor masses. These masses remain for a time on the surface and actually form a partial film between the surface and the liquid. Beyond point D a stable vapor film has covered the entire surface (1). When attempts are made in the complete film boiling region to exceed the heat transfer rate which can be obtained at point C, the surface material usually melts. For this reason point C is often called the "burnout" point.

In recent engineering designs high heat transfer rates have been required. A propellant cooled rocket nozzle is an example of this type of design. Information on boiling heat transfer is needed for the successful development of such equipment. The kind of information most useful to the engineer would perhaps consist of a correlation of the burnout point as a function of parameters characterizing the liquid and the flow field. Attempts at obtaining such a relation have, however, not been successful so far, and it is felt that further study of the mechanism of boiling heat transfer is required before satisfactory relations of this type can be derived.

One may wish to divide the nucleate boiling heat transfer problem into three parts: nucleation of bubbles, bubble motion, and finally the effect of bubbles on heat transfer. This paper is concerned with the last of these aspects.

It has been well established that the bubbles act to increase the heat transfer rate between the surface and the liquid (1, et al.). There are several mechanisms which one could postulate to explain this improvement (1). One suggestion, made by Dr. H. S. Tsien has been that - at least for boiling heat transfer with forced convection - the bubbles act much in the same way as roughnesses. It is then believed that the improvement in heat transfer is the same as that which could be obtained without boiling with a pipe with equivalent roughness elements. If this were the case, one would expect the friction coefficient to increase as the heat transfer coefficient increases. It was the purpose of the tests reported herein to investigate the relationship between these two coefficients.

II. STATEMENT OF PROBLEM

As previously stated, the purpose of the present investigation was to determine any relationship which may exist between the friction coefficient (C_F) and the heat transfer coefficient (C_H) for nucleate boiling heat transfer. Relationships between these two coefficients have been developed on the basis of Reynolds' analogy for several cases of pipe flow (3, 4). If the Prandtl number of the fluid in question is unity this relationship reduces to the simple equation:

$$\frac{C_F}{2} = C_H \,, \qquad (1)$$

and this equation should hold for rough as well as for smooth pipes (4). If the Prandtl number differs from unity one may still expect Eq. (1) to be applicable, provided the roughnesses are large compared to the laminar boundary layer. The results of the present experiments will be compared to Eq. (1).

The heat transfer from, and the pressure drop along a tube with flowing water, under conditions of nucleate boiling heat transfer, have been previously measured with tubes of 1/4 inch diameter (5). These tubes were so small that the formation of bubbles may have obstructed a large percentage of the internal area of the tube and increased the effective velocity of the water. Without additional information on the velocity, therefore, these pressure drop data could not be used for determining the friction and heat transfer coefficients.

In the present investigation similar experiments were carried out with larger tubes, and an attempt was made to measure the velocity at three locations along the tube by using pitot tubes inserted in

the test section. The pitot tubes were used to measure static pressure as well as velocity. The pitot tubes (or similar static probes) were considered necessary for the static pressure measurements, since it was not known whether wall piezometer orifices would give proper readings in the presence of bubbles. From these measurements it was then intended to compute the friction and heat transfer coefficients.

III. TEST INSTALLATION

A. Test Sections

The test section in which the simultaneous measurements of heat transfer and friction were made (see Fig. 2) consisted of a 43 inch length of 3/8 inch diameter tube, with a wall thickness of 0.010 inch. The tube was made of 304 stainless steel. All heating was done electrically by conducting current through the tube wall. Only 17 3/4 inches of the tube near the downstream end were used for heating, and for measurements. The first part of the tube, corresponding to about 56 diameters, was provided so that an equilibrium velocity profile would be established before any measurements would be taken. Three pitot tubes of 0.058 inch outside diameter were constructed, placed through drilled holes spaced at seven inch intervals along the heating section, accurately positioned at the centerline of the test section and fastened by silver soldering. The pitot tube measuring stations are numbered consecutively in the direction of flow. They will be referred to as stations No. 1, 2 and 3 respectively, throughout the remainder of this paper. For reinforcement a small copper sleeve was placed around each pitot tube at the silver soldered joint. The first tube was placed at approximately five diameters downstream of the beginning of the heating section. Two 3/4 inch diameter copper sleeves approximately four inches long were silver soldered to the test section to serve as a place of attachment for electrodes. Stainless steel male tube fittings on both ends of the heating portion of the test section served to attach the test section into the test piping circuit. A thermal

expansion joint with a Teflon O-Ring was incorporated between the tube fitting and the copper sleeve at the downstream end of the test section. The entrance end of the test section was reinforced with a copper sleeve silver soldered to the test section and machined to make a rounded entrance. This test section was used to measure velocities at three positions and differential pressures across these three positions for various heat transfer rates.

A second test section was similarly constructed with the exception that no pitot tubes were installed. Instead, four 0.031 inch diameter holes were drilled 90^{o} apart in the test section at each of the positions corresponding to the pitot tube pressure pick up positions on the first test section. These side holes at each position were connected by a copper piezometer ring to which a copper tube fitting was soldered. The second test section was necessary in order to determine the pressure drop caused by the presence of the pitot tubes themselves. T his part of the pressure drop had to be subtracted from the readings of the pitot static orifices in order to obtain the net pressure drop caused by the tube walls and the bubbles alone.

Fig. 2 is a photograph of the two test sections showing details of the expansion joint. Fig. 3 is a photograph of a test section which has been cut open to show the placement of a pitot tube.

B. Test Circuit

A diagram of the test circuit is shown in Fig. 4. Two fifty gallon stainless steel tanks were used in the test circuit and were connected to the test section, through flanges, by 3/4 inch stainless

steel tubing. The flanges were electrically insulated by Micarta and Teflon. An auxiliary piping circuit, for circulating the water while heating, was constructed of similar tubing and connected the reservoir tank with a circulating pump. The reservoir tank and the tubing which lead from the reservoir tank to the test section were heat insulated with asbestos sheeting. Compressed nitrogen was used to force distilled water from the reservoir tank upward through the test section into the receiver tank. The test section itself was mounted vertically. Choice of the "blow-down" cycle instead of a continuous pumped cycle, was made in order to take advantage of the inherent relative freedom from pressure fluctuations which is characteristic of the blow-down cycle. The test installation was located in a laboratory of the Heat Transfer Section of the Jet Propulsion Laboratory of the California Institute of Technology.

C. Instrumentation

1. Pressure Transmitters

Five separate differential pressure measurements were made on the test section. They were the static pressure drops from station No. 1 to station No. 2, and from station No. 2 to station No. 3, and the three velocity heads at stations No. 1, No. 2 and No. 3. All of these pressure readings were taken either by the pitot tubes inserted in the test section or through the piezometer holes in the tube wall. The orifices and the tubing in each case offer great resistance to flow because of their small size. In order to obtain satisfactory and rapid response, therefore, it was necessary to

use pressure transmitters which required a minimum of volume change. A strain gage type pressure transmitter manufactured by the Statham Laboratories Company was found suitable for this service, and this type of instrument was used for all five pressure readings. All of the pressure transmitters were calibrated by the Instrument Section of the Jet Propulsion Laboratory and were found to be accurate to less than 1°/o of the reading at 6 inches of mercury in linearity and in hysteresis. The transmitters were connected to the pitot tubes by 1/8 inch copper tubing, and the tubing was electrically insulated from the test section by Teflon gaskets between the tube fittings.

For the test section with the wall piezometer holes, the pressure drop between stations was also determined by means of Statham gages. These particular transmitters were accurate to better than 1°/o of the reading at 2 inches of mercury in linearity and in hysteresis.

The signals from the transmitters were recorded at the central recording station on Leeds and Northrup Speedomax, Type G, self balancing continuous recording potentiometers, the calibration accuracies of which were kept better than 1/2°/o of full scale readings.

2. Temperature Measurements

Five different temperatures were measured at the test section: the bulk temperature of the water entering and leaving the test section, and the temperatures of the tube wall at stations No. 1, No. 2 and No. 3. All measurements were made with

Chromel-Alumel thermocouples. The reference temperature in each case was melting ice. For the measurements of the bulk temperature the hot junctions of two thermocouples were each sealed in thin glass and placed in the water upstream of the inlet and downstream of the outlet of the test section. Two stainless steel screen discs were placed just before the outlet thermocouple to insure thorough mixing of the water. In this case the thermocouple reading is equal to the water average bulk temperature. Fig. 5 shows a photograph of a glass sealed thermocouple in its packing gland unit.

For measurements of the wall temperature, the hot junctions of the thermocouples were clamped against the tube wall. They were electrically insulated from the wall by a 0.0007 inch maximum thickness of mica sheet, and they were separated from the clamp by a layer of natural Sil-O-Cel (see Figs. 2 and 6).

The electrical signals from all the thermocouples were recorded on a Leeds and Northrup Speedomax, Type G, self balancing 16 channel recording potentiometer. The calibration accuracy of this unit was better than $1/2^{o}/o$ of full scale reading.

Fig. 6 is a photograph of the test section as installed. The flange attachments at the outlet of the test section and at the inlet to the heating portion, are for the purpose of electrically insulating the test section from the rest of the piping circuit. The pitot tube stems are shown protruding from the test section. The leads of the wall temperature, thermocouple hot junctions may also be seen. The outlet bulk temperature thermocouple is shown at the top of the photograph, downstream of the flange. In the lower background is

the ice bath for the thermocouple cold junctions. The pressure transmitters are shown to the right center of the photograph. The electrodes from the welding generator power supply are located at the top and bottom of the heating portion of the test section.

3. Power Supply and Additional Equipment

In order to obtain any desired temperature of the test water, it was necessary to be able to heat the water in the reservoir (see Fig. 4) prior to the test. For this purpose two 5 kilowatt General Electric copper immersion heaters were installed in the reservoir tank. In the bottom of the reservoir tank was placed a Weston Thermometer, Model 1221, with a range of 50 - 500° F, so that the temperature of the water could be observed during the heating cycle.

To regulate the pressure in the water reservoir during the discharge cycle, a Grove Loader with a Grove Dome Controller was used. The compressed nitrogen was supplied from the central system of the laboratory.

The large amount of current for the test section itself was obtained from two Hobart Simplified Arc Welders connected in parallel. Each welder had a maximum current capacity of 600 amperes and a voltage rating of 40 volts. The voltage drop across the test section was measured by a Weston D. C. Voltmeter, Model 622, and the current was measured by a Weston D. C. millivoltmeter, Model 622, in conjunction with a 2000 ampere, 50 millivolt shunt. Both meters were accurate to 1/2°/o of the full scale reading. The shunt resistance was accurate to $\pm$ 1/2°/o.

The water mass flow rate was obtained from a 1/4 inch throat diameter Venturi flowmeter constructed at the Jet Propulsion

Laboratory. The differential pressure between the venturi throat static pressure and the total pressure was recorded on a Barton Hydraulic Rotary Recorder, Model 202, with a range of 0 - 300 inches of water. The gage and Venturi flowmeter were calibrated together as a unit and the calibration is shown in Fig. 7.

An Ashcroft Laboratory Test Gage, range 0 - 300 psi, calibrated to better than 1/2^{o}/o accuracy of full scale reading, was used to read the pressure in the heating tank during the test run.

The water mass flow rate was hand controlled by a 3/4 inch Vogt stainless steel metering valve.

IV. TEST PROCEDURE

Tests were made with both test sections for each of the three pressure levels, 265, 115 and 65 psia, for a mass flow rate of approximately 0.75 pounds per second and for heat transfer rates ranging from 0.0 to a maximum of approximately 2.1 Btu/sq in-sec.

Prior to a run, distilled water in the reservoir was heated to the desired temperature by the immersion heaters. This temperature was selected to be approximately 100°F below the saturation value for each pressure. Occasionally the water was circulated by the circulating pump to insure uniform temperature. When the water was at the predetermined temperature, compressed nitrogen was introduced to the reservoir. The nitrogen pressure was maintained at the desired value throughout the test run by means of the regulator. The throttle valve was opened and adjusted to pass the predetermined flow rate. The welding generators were then turned on and the power input to the test section was varied in steps. During each run, the temperature of the water entering and leaving the test section as well as the three outside wall temperature measurements were recorded. Simultaneously the velocity was measured at the three stations and the differential pressure between stations was taken. Prior to emptying the reservoir of water, electric power to the test section was turned off so as to avoid burnout. The water in the receiver tank was pumped back into the reservoir in preparation for the next run.. A similar testing procedure was used when the second test section was installed, except that velocity and wall temperature measurements were omitted.

V. DESCRIPTION OF MEASUREMENTS AND COMPUTATIONS

A. Test Section Measurements

The physical measurements of the test sections which were used in the computations are tabulated in Appendix B. The outside diameter (d_o) and the wall thickness (w_t) were measured at several places near the entrance and exit of the test sections and averaged. See Appendix A for a complete list of symbols.

B. Flowmeter Calibration

The Venturi flowmeter and the associated pressure gage were calibrated together for different gage pressures (see Fig. 7) by flowing water at a temperature of 170°F from the reservoir tank through the Venturi flowmeter into a tank placed on a platform scale. The time for a given weight discharge was measured. Since the Venturi flowmeter was calibrated for only one water temperature, the mass flow rate (m) had to be corrected for changes in water temperature, and consequently in density (ρ).

C. Heat Balance

A heat balance was made for most of the test runs by comparing the rise in bulk temperature (Δt_b) of the water through the test section, as computed from power measurements, with the actual rise. The computed temperature rise was obtained from the equation:

$$\Delta t_b = \frac{P}{mC} \times \frac{3.413}{3600} \quad {}^{o}F, \tag{2}$$

where P is the electrical power in watts, m is given in lbs/sec and C is the heat capacity of the water in Btu/lb-°F. The actual bulk

temperature rise in the test section was determined by taking the difference of the water bulk temperature at the inlet and outlet of the test section. Figs. 8, 9 and 10 are graphs of the actual and computed bulk temperature rise for test section pressure levels of 265, 115 and 65 psia, respectively, for various heat transfer rates (q/A) in Btu/sq in-sec. Only for the runs at 265 psia pressure was there any detectable heat loss to the surrounding atmosphere. The loss was approximately 4-1/2°/o. Figures based on the actual bulk temperature rise were used in computing heat transfer rates.

D. Wall Temperature

The temperature of the outside wall of the test section was taken at stations No. 1, No. 2 and No. 3. Figs. 11, 12 and 13 show a graph of these temperatures for various heat transfer rates at various pressures. The temperature of the inside wall (t_{wi}) adjacent to the water in the test section was determined by subtracting the temperature drop through the wall (Δt_w) from the temperature of the outside wall (t_{wo}). The temperature drop through the wall was calculated from the equation (6):

$$\Delta t_w = \frac{q}{A} \frac{w_t}{K_w} \left[\frac{1}{2} + \frac{w_t}{6d_o}\right] \frac{3600 \times 144}{12} \quad {}^{o}F, \tag{3}$$

where q/A is given in Btu/sq in-sec, w_t and d_o are given in inches and K_w is the thermal conductivity in $\frac{\text{Btu}}{\text{ft-hr-}^{o}\text{F}}$ (see Fig. 14). This equation was derived by assuming uniform heating throughout the tube wall and no heat flow to the outside.

E. Detection of Incipient Boiling

A graph was made of the outside wall temperature at each of the three stations (see for example Fig. 15) on semi-log paper for various heat transfer rates. At the start of boiling the slope of these curves changes abruptly. The curves were used to determine which of the tests were actually conducted in the nucleate boiling region. As can be seen from the figure, boiling started at all three stations in the heat transfer range between 1.0 and 1.5 Btu/sq in-sec for a pressure level of 115 psia. Boiling was also found to start within the same range for the pressure levels of 265 and 65 psia.

F. Velocity Measurements

Velocity measurements were taken at the centerline of the test section and graphs of the measurements are shown in Figs. 16, 17 and 18. The absolute values of the velocities at stations No. 2 and No. 3, are not considered reliable since they were influenced by the wake of the preceding pitot tube or tubes. The change of the velocity readings with increasing heat transfer rate, however, was taken as an indication of the change in average velocity at the station in question. This method of computing the average velocity was based on the assumption that the ratio of the velocity at the center of the test section to the average velocity remains unaffected by the rate of heat transfer as well as by the bubbles on the wall. This assumption is believed to be adequate in view of the fact that the correction involved is small. The variation in velocity between measuring stations was taken as linear.

G. Pressure Drop

For the first test section the pressure drop between stations was determined by measuring the difference in static pressure between the three pitot tubes. Graphs were made of the pressure drops for the three pressure levels, 265, 115 and 65 psia, for various heat transfer rates, and for various initial water bulk temperatures (t_{bi}) (see Figs. 19 to 24). These pressure drop measurements, however, are not yet the required ones since they include a loss which is due to the presence of the pitot tubes themselves. This loss must be subtracted from the data obtained from the first test section. For this purpose similar pressure drop measurements were made along a second test section constructed without pitot tubes, but with wall piezometer holes. These pressure drop measurements were made for heat transfer rates in the non-boiling region only (see Figs. 19 to 24), as the wall pressures could not be considered reliable in the boiling region. The difference between the two sets of pressure measurements was taken as the pressure loss caused by the pitot static tubes. For any given pressure level this loss was assumed to remain constant over the whole range of heat transfer rates investigated. The pressure loss caused by the pitot tubes was then subtracted from the measurements obtained with the first test section. Curves of pressure drop versus heat transfer rate adjusted in this manner are shown in Figs. 25 to 30.

H. Friction Coefficient

The friction coefficient is defined by the equation:

$$C_F \frac{1}{2} \frac{\rho}{g} \overline{V}^2 = \tau_o , \tag{4}$$

where τ_o is the fluid shear on the tube wall and $\overline{V}$ is the average velocity. Writing a force balance for a fluid flowing steadily in a tube this coefficient can be related to the pressure gradient as follows:

$$C_F \frac{1}{2} \frac{\rho \overline{V}^2 \pi d'}{g} = - \frac{dp}{dx} \frac{\pi d'^2}{4} 1728 , \tag{5}$$

where ρ is given in lbs/ft^3, $\overline{V}$ is given in ft/sec, d' is the effective inside diameter, g is the acceleration of gravity in ft/sec^2, $\frac{dp}{dx}$ is the corrected pressure gradient along the test section in lbs/in^3. The average velocity $\overline{V}$, and the diameter d', can be related to the mass flow by the equation:

$$\frac{\pi d'^2}{4} \rho \overline{V} = m. \tag{6}$$

Substituting this expression into Eq. (5), one obtains for C_F the relation:

$$C_F = - \frac{dp}{dx} \frac{gm}{\overline{V}^{5/2} \rho^{3/2}} \frac{1728}{\pi^{1/2}} . \tag{7}$$

To determine the gradient $\left(\frac{dp}{dx}\right)$, the data shown in Figs. 25 to 30 were used to construct a graph of pressure versus distance along the test section, for three constant heat transfer rates. For this graph the pressure at station No. 1 (x = 0 position) was taken equal to the pressure in the reservoir tank, the pressure at station No. 2 (x = 7 inches) was obtained by subtracting the amount of the pressure drop between stations No. 1 and No. 2 (Δp_{1-2}) from the pressure at station No. 1, and the pressure at station No. 3

(x = 14 inches) was obtained by further subtracting the pressure drop between stations No. 2 and No. 3. Figs. 31 to 33 show the pressure distributions along the test section for heat transfer rates of 1.0, 1.5 and 2.0 Btu/sq in-sec for each of three pressure levels in the reservoir tank, 265, 115 and 65 psia. To determine the pressure gradient ($\frac{dp}{dx}$), it was assumed that the graphs of Figs. 31 to 33 were segments of a parabola, whose equation is of the form:

$$p = a + bx + cx^2. \tag{8}$$

The equation was written for each of the three positions x = 0, 7 and 14 inches and solved simultaneously to determine the constants. The derivative,

$$\frac{dp}{dx} = b + 2cx, \tag{9}$$

was used to determine $\frac{dp}{dx}$ at the desired value of x. The local water density was of course used for ρ. The value of $\overline{V}$ was obtained by dividing the mass flow rate by the initial water density and the cross-sectional area of the tube, and by adjusting this value for any velocity increase indicated by the pitot tube readings (see Section V-F). The value of m was obtained from the flowmeter data.

J. Heat Transfer Coefficient

The heat transfer coefficient is defined for steady flow of liquid through a tube as:

$$C_H = \frac{144 \frac{q}{A}}{\rho C \overline{V}(t_{wi} - t_b)}, \tag{11}$$

where the heat capacity (C) is given in Btu/lb-^{o}F.

The heat transfer rate (q/A) was determined from the relation:

$$\frac{q}{A} = \Delta t_b \frac{mC}{A} \quad \text{Btu/sq in-sec,} \tag{12}$$

where Δt_b is the observed actual bulk temperature rise in the water through the test section (see Figs. 11 to 13), and A is the area in sq in of the heating surface of the test section, based on the actual inside diameter. The values of ρ and of $\overline{V}$ are the same as those used for the equation for C_F (Eq. 7). The temperature difference $(t_{wi}-t_b)$ was obtained by subtracting from the value of the outside wall temperature the change of temperature through the test section wall (see Eq. 3) and the bulk temperature of the water in the test section.

VI. PRESENTATION OF RESULTS

A. Velocity Measurements

Figs. 16 to 18 show the results of the velocity measurements at the three stations along the test section. The measurements were taken at pressure levels of 265, 115, and 65 psia, and they covered a heat transfer range from 0.0 to 2.1 Btu/sq in-sec. The velocity measurements were constant at station No. 1 for all three pressures. This was to be expected considering that station No. 1 was only 1.7 inches downstream of the point where heating started. The subcooling was still large, and under that condition the bubbles were small, as was shown by Gunther (2). The flow velocity at stations No. 2 and No. 3 increased somewhat with increase in heat transfer. This increase became noticeable at about 1.0 to 1.5 Btu/sq in-sec, which was the heat transfer rate at which boiling was determined to have begun (see Section V-E). The flow velocity at station No. 3 was affected more than that at station No. 2. This result may be explained by the difference in subcooling at the two stations. It is also interesting to note that at high heat transfer rates, the velocity at station No. 3, became rather sensitive to the bulk temperature of the water at the inlet to the test section. This again is believed to be due to the reduced subcooling which resulted from higher inlet temperatures.

As mentioned before, the absolute values of the measured velocity at stations No. 2 and 3 are not considered significant because of the wake of the preceding pitot tube or tubes. The change in velocity with boiling is, however, believed to be indicative of the increase in the average velocity, and the average velocity was corrected accordingly, as discussed in Section V-F.

B. Pressure Measurements

Results of the pressure drop measurements are shown in Figs. 19 to 24. These figures show the results for the test section with pitot tubes installed and at pressure levels of 265, 115 and 65 psia. The pressure drop was plotted as a function of the heat transfer rate, and values of the water bulk temperature at the inlet to the test section are indicated. Figs. 19 to 24 also show similar results for the test section without pitot tubes. For the test section with pitot tubes installed, the range of heat transfer rates investigated was from 0.0 to 2.0 Btu/sq in-sec, and for the test section without pitot tubes, 0.0 to 1.2 Btu/sq in-sec. The pressure drop was observed to increase with an increasing heat transfer rate in all cases after boiling started. The increase was greater between stations No. 2 and No. 3 than between stations No. 1 and No. 2. This result can again be related to the reduction in subcooling along the test section. The effect of the inlet water bulk temperature may be explained similarly. In the non-boiling region the pressure drop was observed to decrease slightly with increasing heat transfer rate. This is probably due to viscosity changes near the tube wall during heating.

Figs. 31, 32 and 33 represent the same pressure data as discussed in the previous paragraph, except that they have been adjusted for the pressure loss caused by the pitot tubes as explained in Section V-G.

Finally using the measurements discussed in the foregoing, the friction and heat transfer coefficients were computed as outlined in Sections V-H and V-J. The results are presented in two

graphs, a graph of the friction coefficient (C_F) versus the heat transfer rate (q/A) for various pressure levels (Fig. 34), and a graph showing the relationship between one-half the friction coefficient and the heat transfer coefficient (Fig. 35). The graphs will be discussed in the following section.

VII. CONCLUSIONS

The fact that nucleate boiling improves the heat transfer rate is well known (1, 2, et al.). The purpose of the present investigation was to determine the effect of nucleate boiling on fluid friction for a forced convection system. In particular it was desired to determine whether any relationship exists between friction and heat transfer for water flowing through a tube. For the comparison, the heat transfer and friction coefficients were chosen rather than the overall pressure drop and heat transfer rates. In this manner it was possible to exclude any effects caused simply by changes in the flow velocity or in the temperature differential between the tube wall and the water.

Fig. 34 is a graph of the friction coefficient versus the heat transfer rate. The points shown were taken at constant subcooling, and at an average pressure of 115 psia. The point at which boiling began has been indicated. It can be seen that with increasing heat transfer rate the friction coefficient actually increases. This shows that the increase in pressure drop (see Figs. 25 to 30) cannot be explained solely by an increase in the effective velocity which might have been caused by an obstruction of the flow passage by the bubbles. The rise in the friction coefficient indicates that the bubbles actually influence the momentum exchange. The simultaneous effect of the bubbles on the heat transfer can be examined by considering a graph of one-half the friction coefficient ($\frac{C_F}{2}$) versus the heat transfer coefficient (C_H). Such a graph is shown in Fig. 35. The results shown were taken at three different pressure levels,

for a heat transfer range from 1.0 to 2.0 Btu/sq in-sec and for various degrees of subcooling. It can be seen that the experimental points define as an average curve, a line given approximately by the equation:

$$\frac{C_F}{2} = C_H \,. \tag{1}$$

This, however, is the relationship which is obtained from Reynolds' analogy either for the case where a laminar boundary layer at the heating surface is non-existent or for the case where the Prandtl number for the fluid is equal to 1.0. The Prandtl number of water varied between 1.0 and 2.0 for the range of bulk temperatures investigated. As the Prandtl number of the fluid was relatively close to one, the question of whether or not the laminar boundary layer existed will have to be left undecided. In view of the results shown in Fig. 35, it can, however, be stated that the bubbles affect the heat transfer and the friction in the "same way", within the meaning of Reynolds' analogy. It appears, therefore, that the effect of the bubbles is a purely hydrodynamic one, acting on the turbulent exchange coefficients both for friction and for heat transfer. Thus the results of the present experiments seem to be in agreement with Tsien's hypothesis which was mentioned in Section I.

In conclusion, it should be pointed out that the experiments covered only a rather limited range of Reynolds numbers (140,000 to 380,000) and that the flow velocities were in all cases higher

than the average bubble growth rates. At lower velocities and different Reynolds numbers, the nucleate boiling may have a different effect. This should certainly be true for boiling under free convection conditions, because in that case the bubble growth velocities must have a strong influence on the flow field.

REFERENCES

1. Ellion, M. E., A Study of the Mechanism of Boiling Heat Transfer, Thesis, Calif. Inst. Tech., 1953.

2. Gunther, F. C., Photographic Study of Surface-Boiling Heat Transfer to Water with Forced Convection, Trans. ASME, Vol. 73, 1951, pp. 115-123.

3. von Karman, T., The Analogy Between Fluid Friction and Heat Transfer, Trans. ASME, Vol. 61, 1939, pp. 705-710.

4. Martinelli, R. C., Heat Transfer to Molten Metals, Trans. ASME, Vol. 69, 1947, pp. 947-959.

5. Buchberg, H., et al., Studies in Boiling Heat Transfer, AEC Final Rpt. Contr. No. AT 11-1-Gen-9, Univ. Calif., L.A., Mar. 1951.

6. McAdams, W. H., Addoms, J. N., and Kennel, W. E., Heat Transfer at High Rates to Water with Surface Boiling, Rpt. No. ANL-4268, Mass. Inst. Tech., Dec 1948.

7. Hogan, C. L., The Thermal Conductivity of Metals at High Temperature, Bell Aircraft Corp. Rpt. No. 56-982-010, Oct. 1, 1950.

APPENDIX A

Nomenclature

A	Heating area of test section based on length and inside diameter of heating section	sq in
C	Heat capacity of water	Btu/lb-^{o}F
C_F	Friction coefficient	
C_H	Heat transfer coefficient	
K_w	Thermal conductivity of stainless steel	Btu/ft-hr-^{o}F
P	Electrical power	watts
V	Velocity as measured by pitot tubes	ft/sec
$\overline{V}$	Average velocity	ft/sec
a, b, c	Coefficients	
d'	Effective inside diameter of test section	in
d_i	Actual inside diameter of test section	in
d_o	Outside diameter of test section	in
g	Acceleration of gravity	ft/sec^2
m	Water mass flow rate	lbs/sec
p	Water pressure	psia
q/A	Heat transfer rate	Btu/sq in-sec
t_b	Bulk temperature of water	^{o}F
t_{bi}	Bulk temperature of water initially (i.e. at inlet to test section)	^{o}F
t_{wi}	Temperature of inside wall of test section	^{o}F
t_{wo}	Temperature of outside wall of test section	^{o}F
w_t	Test section wall thickness	in
x	Distance downstream from station No. 1 (see Fig. 3)	in

Δp	Pressure drop between stations noted in subscript	psi
Δt_w	Temperature drop through test section wall	^oF
ρ	Density of water	lbs/ft^3

Subscripts 1, 2, 3 — At stations No. 1, 2, 3

APPENDIX B

Dimensions

Test Section with Pitot Tubes Installed:

Outside Diameter (d_o)	0.3786 in
Wall Thickness (w_t)	0.0103 in
Inside Diameter (d_i)	0.3580 in
Length of Heating Section	17.75 in
Heating Area (A), based on Inside Diameter	19.95 sq in
Diameter of Pitot Tubes	0.058 in

Test Section without Pitot Tubes:

Outside Diameter (d_o)	0.3783 in
Wall Thickness (w_t)	0.0103 in
Inside Diameter (d_i)	0.3577 in
Length of Heating Section	17.75 in
Heating Area (A), based on Inside Diameter	19.93 sq in

APPENDIX C

Sample Computations

For the sample computations, a particular run at a test section pressure level of 265 psia, with a heat transfer (q/A) of 2.0 Btu/sq in-sec, is here considered. The inlet bulk temperature (t_{bi}) for this run was 307°F. The coefficients are computed for a point where the subcooling was 80°F. At the given pressure, 80°F subcooling corresponds to a bulk water temperature (t_b) of 326°F.

Friction Coefficient (C_F):

The pressure variation along the test section is assumed to be of the form,

$$p = a + bx + cx^2. \tag{8}$$

Using the experimental values at x = 0, 7 and 14 inches with the aid of Figs. 25 and 26, the coefficients are obtained by means of the following three equations:

$$265.0 = a$$

$$264.35 = a + 7b + 49c$$

$$263.53 = a + 14b + 196c.$$

When solved simultaneously, one obtains:

$$b = -0.0807,$$

and

$$c = -0.001735.$$

The gradient,

$$\frac{dp}{dx} = b + 2cx, \tag{9}$$

is found to be:

$$\frac{dp}{dx} = -(0.0807 + 0.00347x).$$

The value of x (see Fig. 3) is determined by simple proportioning from a consideration of the actual bulk temperature rise in the test section (see Fig. 8) and of the length of the test section (see Appendix B). In this way, x is determined to be equal to 4.9 inches. Then,

$$\frac{dp}{dx} = 0.0977 \text{ lbs/in}^3,$$

At the test section entrance the average velocity ($\overline{V}$) of the water is given by:

$$\overline{V} = \frac{4m \times 144}{\rho \pi d'^2}, \tag{6}$$

where d' is in this case the actual inside diameter (d_i) of the test section.

$$d_i = d' = 0.3580 \text{ in},$$

$$m = 0.73 \text{ lbs/sec}$$

and

$$\rho = 57.0 \text{ lbs/ft}^3,$$

$$\overline{V} = \frac{4 \times 0.73 \times 144}{57.0 \times 3.14 \times 0.3580^2} = 18.3 \text{ ft/sec},$$

but $\overline{V}$ must be evaluated at x = 4.9 in. From Fig. 16 it can be seen that the velocity at station No. 2 must be corrected by the ratio of $\frac{21.1}{20.7}$. There is no observable increase in the measured velocity

at station No. 1, so no correction is made to the average velocity there. By linear interpolation to the value of x between the two stations,

$$\overline{V} = 18.6 \text{ ft/sec.}$$

The friction coefficient is given by:

$$C_F = \frac{dp}{dx} \frac{g\, m^{1/2}\, 1728}{\overline{V}^{5/2}\, \rho^{3/2}\, \pi^{1/2}} . \tag{7}$$

Therefore,

$$C_F = \frac{0.0977 \times 32.2 \times 0.73^{1/2} \times 1728}{18.6^{5/2} \times 56.5^{3/2} \times 3.14^{1/2}} = 0.0041$$

Heat Transfer Coefficient (C_H):

Δt_b (actual) = 51°F (see Fig. 8),

A = 19.95 in (see Appendix B)

and

C = 1.04 Btu/lb-°F.

The effective heat transfer rate (q/A) is given by:

$$\frac{q}{A} = \Delta t_b \frac{mC}{A} . \tag{12}$$

$$\frac{q}{A} = \frac{51 \times 0.73 \times 1.04}{19.95} = 1.94 \text{ Btu/sq in-sec.}$$

The temperature of the outside wall (t_{wo}) is obtained from Figs. 11 and 12 with linear interpolation between stations.

$$t_{wo} = 475^{\circ}\text{F.}$$

The temperature drop (Δt_w) through the test section wall is given by (6):

$$\Delta t_w = \frac{q}{A} \frac{w_t}{K_w} \left[\frac{1}{2} + \frac{w_t}{6 d_o} \right] \frac{3600 \times 144}{12} , \tag{3}$$

where $\dot{q}/A$ = 2.0 Btu/sq in-sec, since Eq. (3) was derived on the assumption of no heat loss to the surroundings.

$$d_o = 0.3786 \text{ in,}$$

and

$$w_t = 0.0103 \text{ in (see Appendix B).}$$

$$K_w = 13.2 \text{ Btu/ft-hr-}^{\circ}\text{F (see Fig. 14).}$$

Therefore

$$\Delta t_w = 2 \frac{0.0103}{13.2} \left[\frac{1}{2} + \frac{0.0103}{6 \times 0.3786} \right] \frac{3600 \times 144}{12} = 33^{\circ}\text{F.}$$

$$t_{wi} - t_b = 475^{\circ} - (33^{\circ} + 326^{\circ}) = 116^{\circ}\text{F.}$$

The heat transfer coefficient (C_H) is given by:

$$C_H = \frac{144 \frac{q}{A}}{\rho C \overline{V} (t_{wi} - t_b)} \qquad (11)$$

Therefore,

$$C_H = \frac{144 \times 1.94}{56.5 \times 1.04 \times 18.6 \times 116} = 0.0022.$$

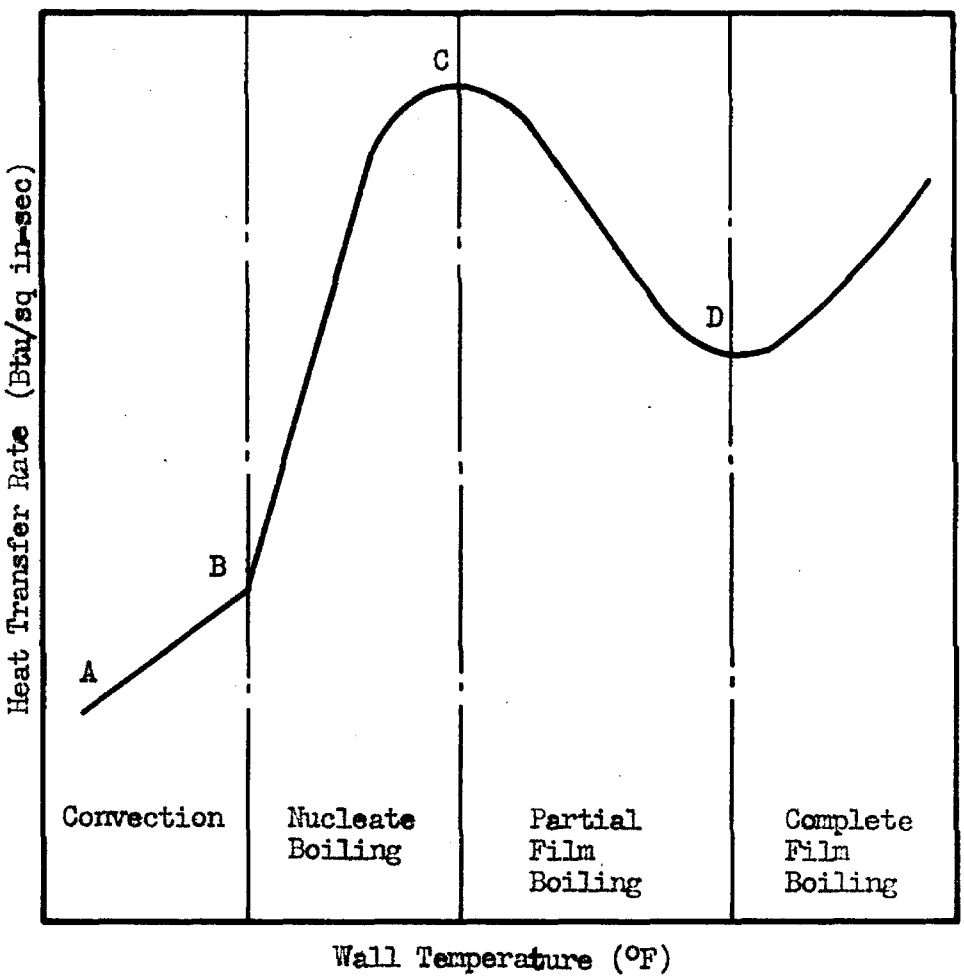

Fig. 1 Typical Heat Transfer Curve (1)

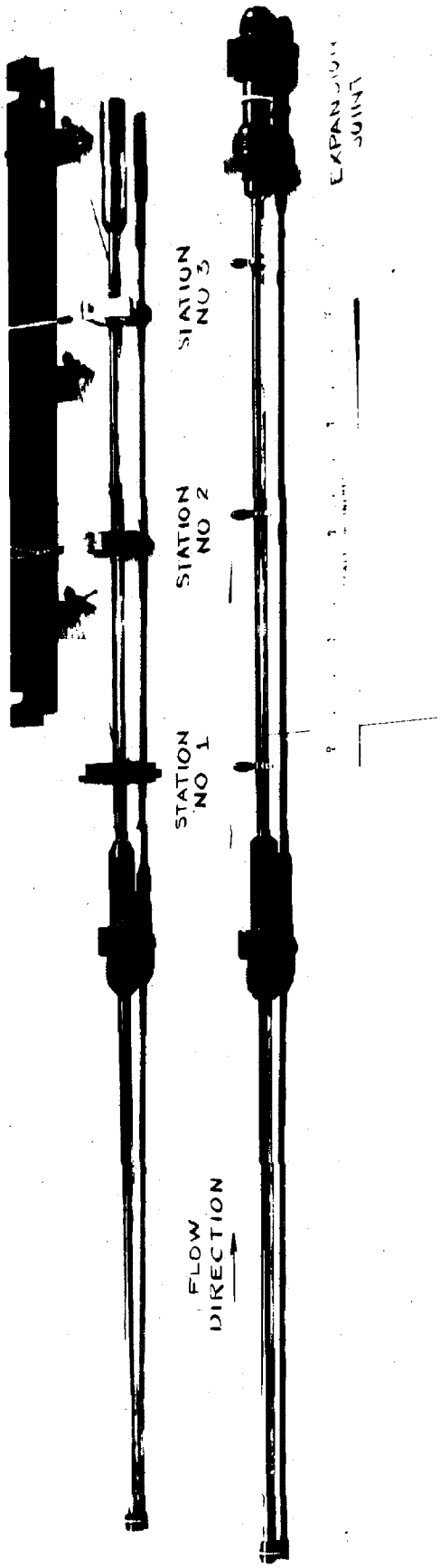

Fig. 2 Photograph of Test Sections

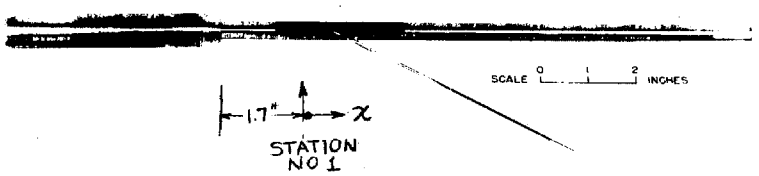

Fig. 3 Photograph of Pitot Tube Installed in Test Section

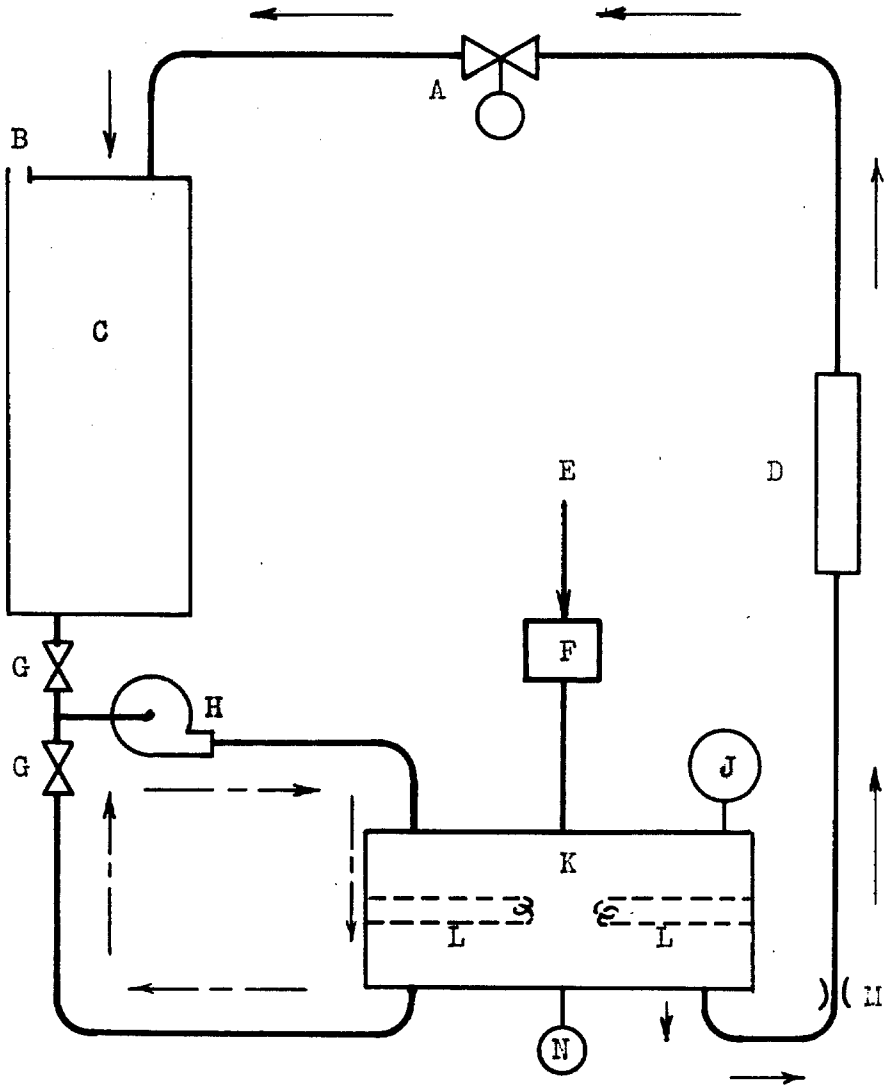

Test Cycle Flow Path
Heat Cycle Flow Path

A	Throttle Valve	H	Circulating Pump
B	Vent	J	Pressure Gage
C	Receiver Tank	K	Reservoir Tank
D	Test Section	L	Immersion Heater
E	Compressed Nitrogen	M	Venturi Flowmeter
F	Pressure Regulator	N	Thermometer
G	Valve		

Fig. 4 Test Circuit Diagram

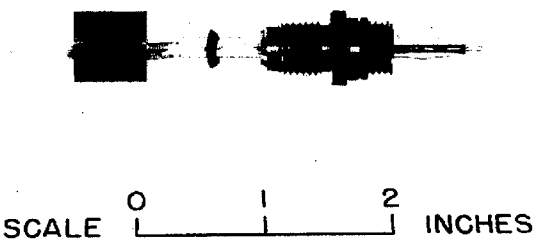

Fig. 5 Photograph of Glass Sealed Thermocouple with Packing Gland

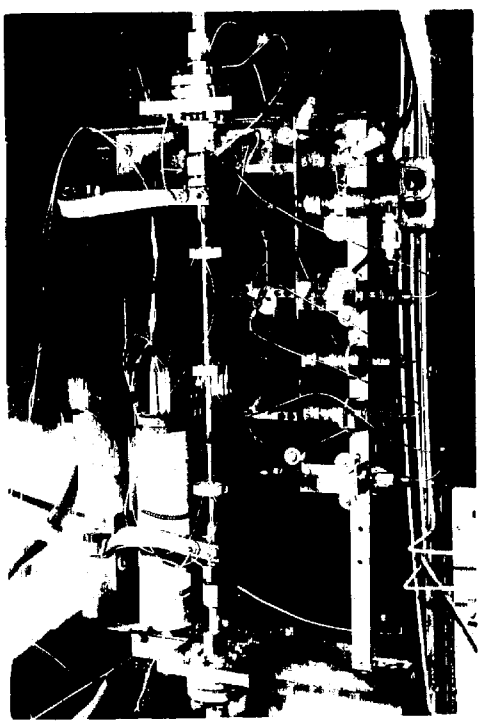

Fig. 6 Photograph of Test Section Installation

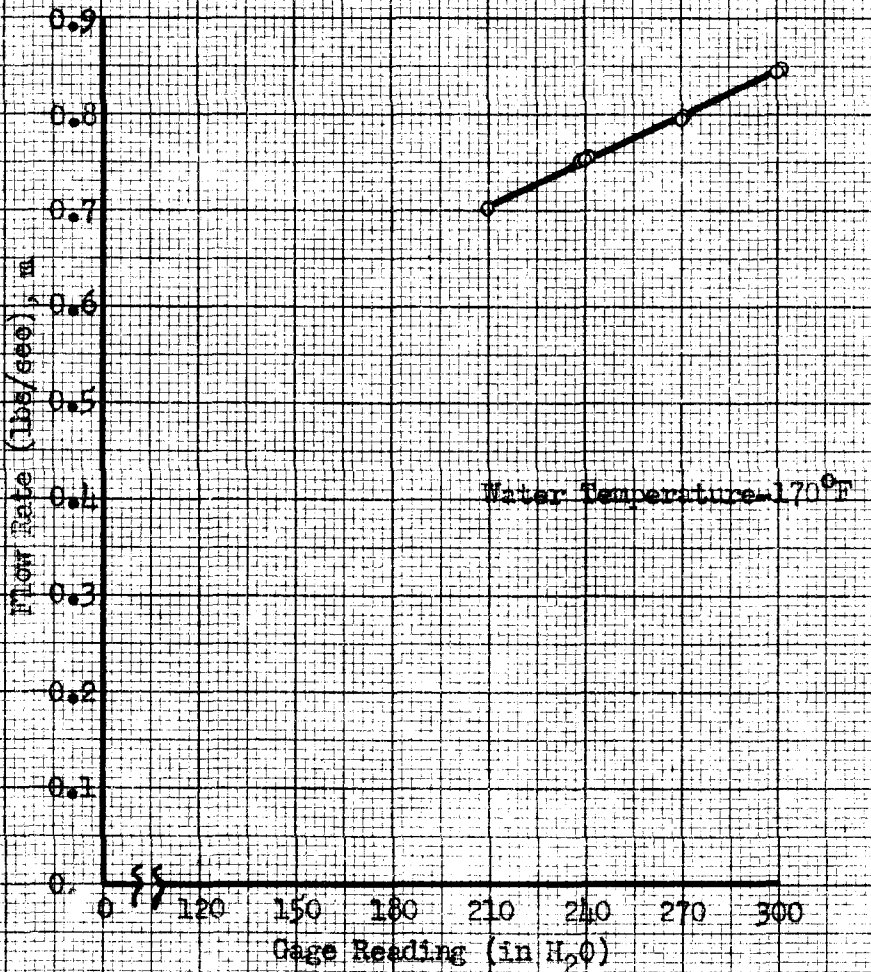

Fig. 7 Venturi Flowmeter and Pressure Gage Calibration

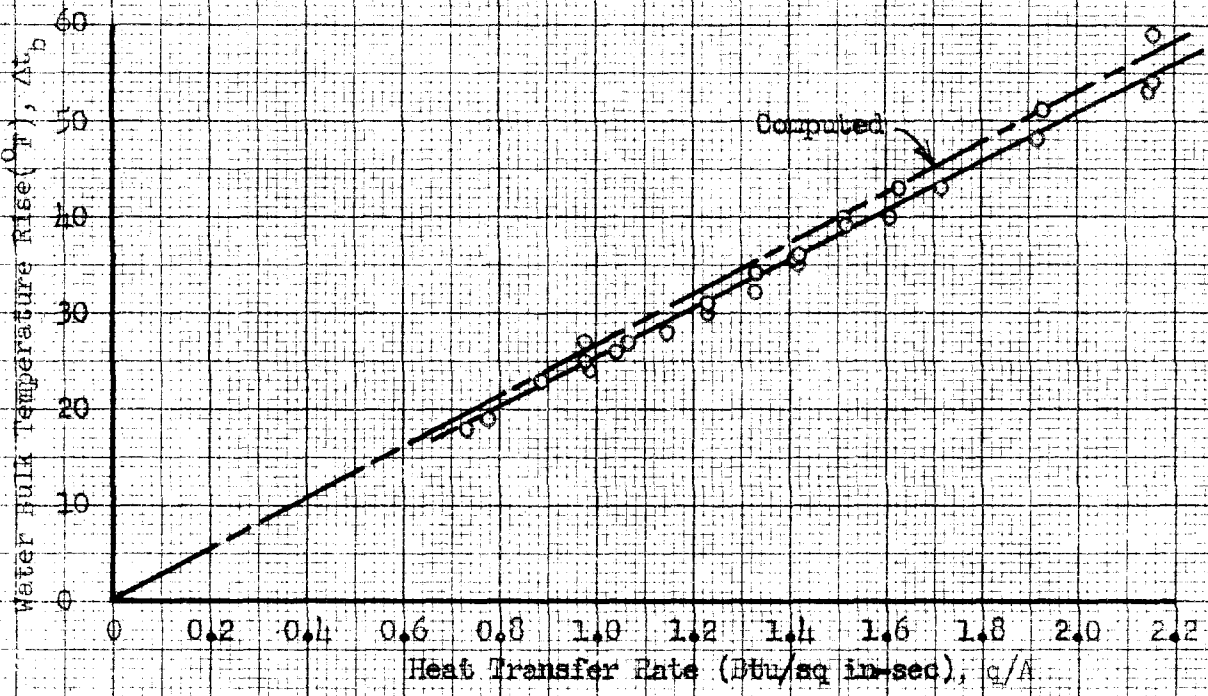

Fig. 8 Actual and Computed Water Bulk Temperature Rise vs Heat Transfer Rate for a Test Section Pressure of 265 psia

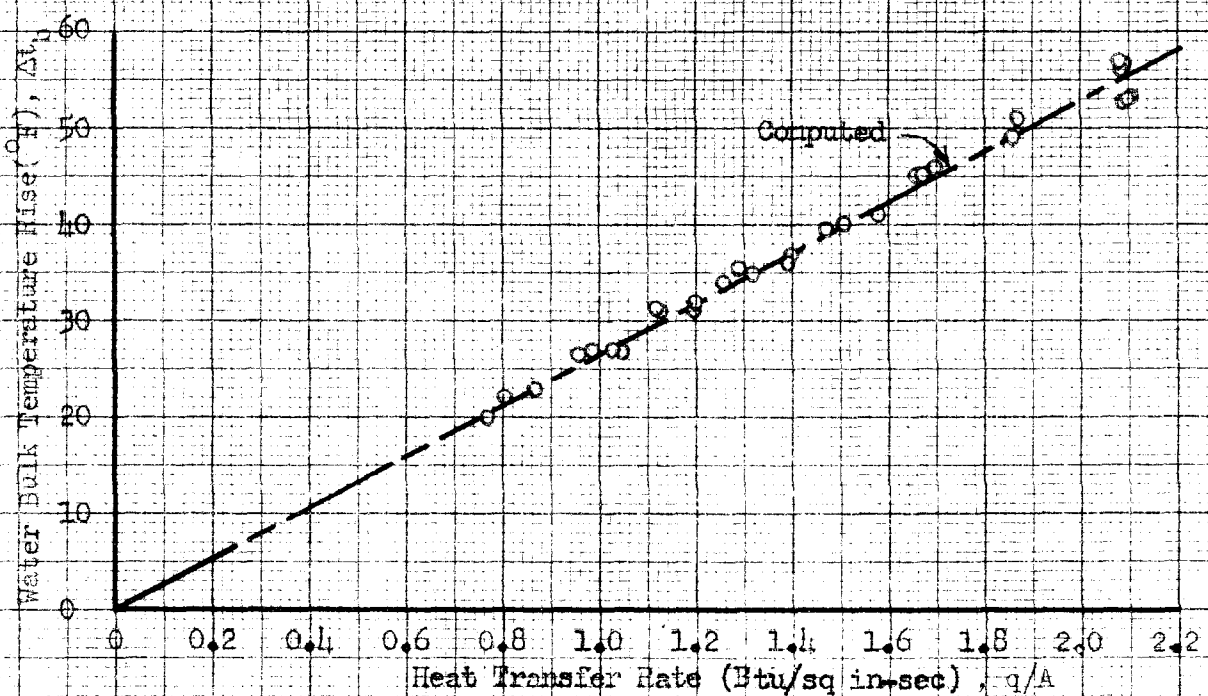

Fig. 9 Actual and Computed Water Bulk Temperature Rise vs Heat Transfer Rate for a Test Section Pressure of 115 psia

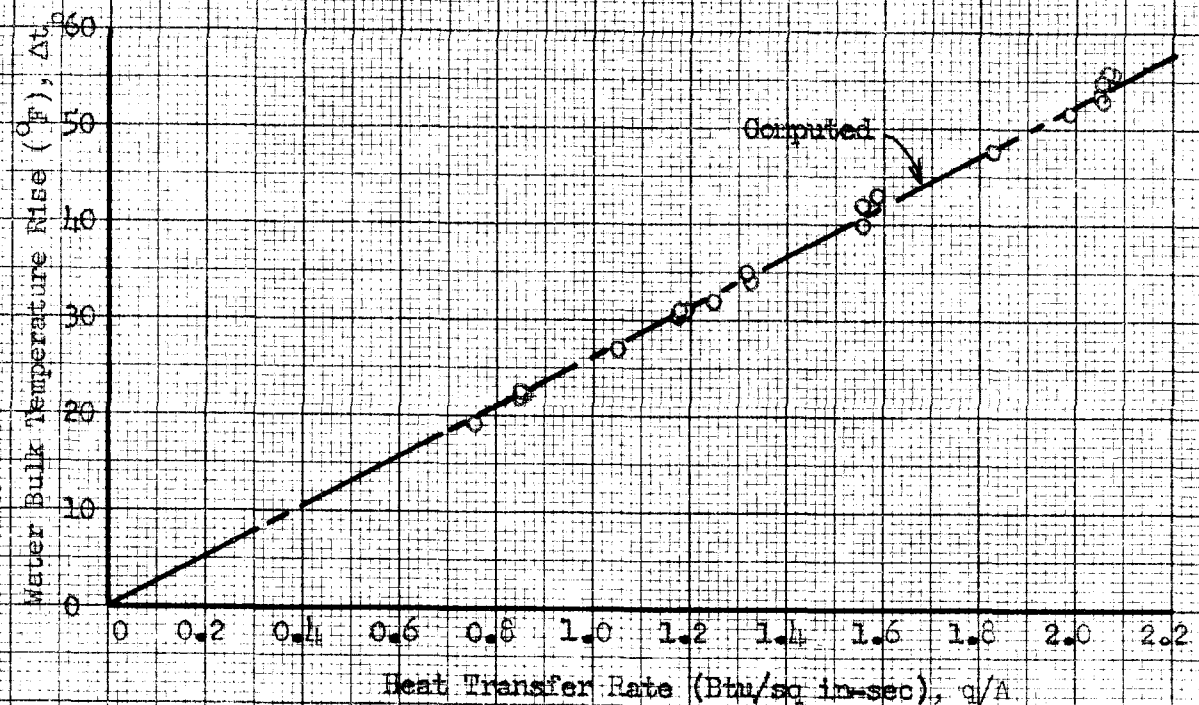

Fig. 10 Actual and Computed Water Bulk Temperature Rise vs Heat Transfer Rate for a Test Section Pressure of 65 psia

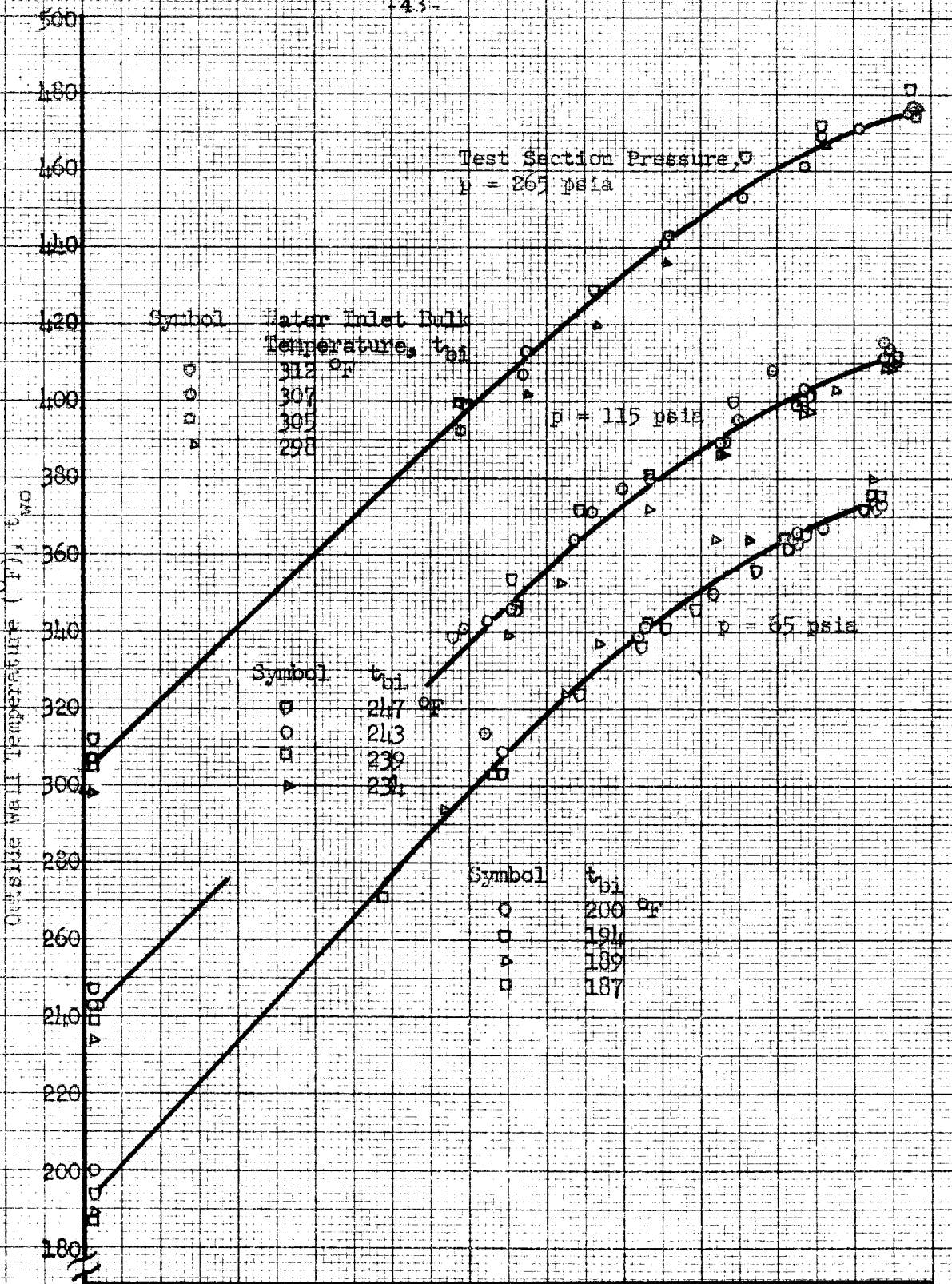

Fig. 11 Outside Wall Temperature of Test Section at Station No. 1 vs Heat Transfer Rate

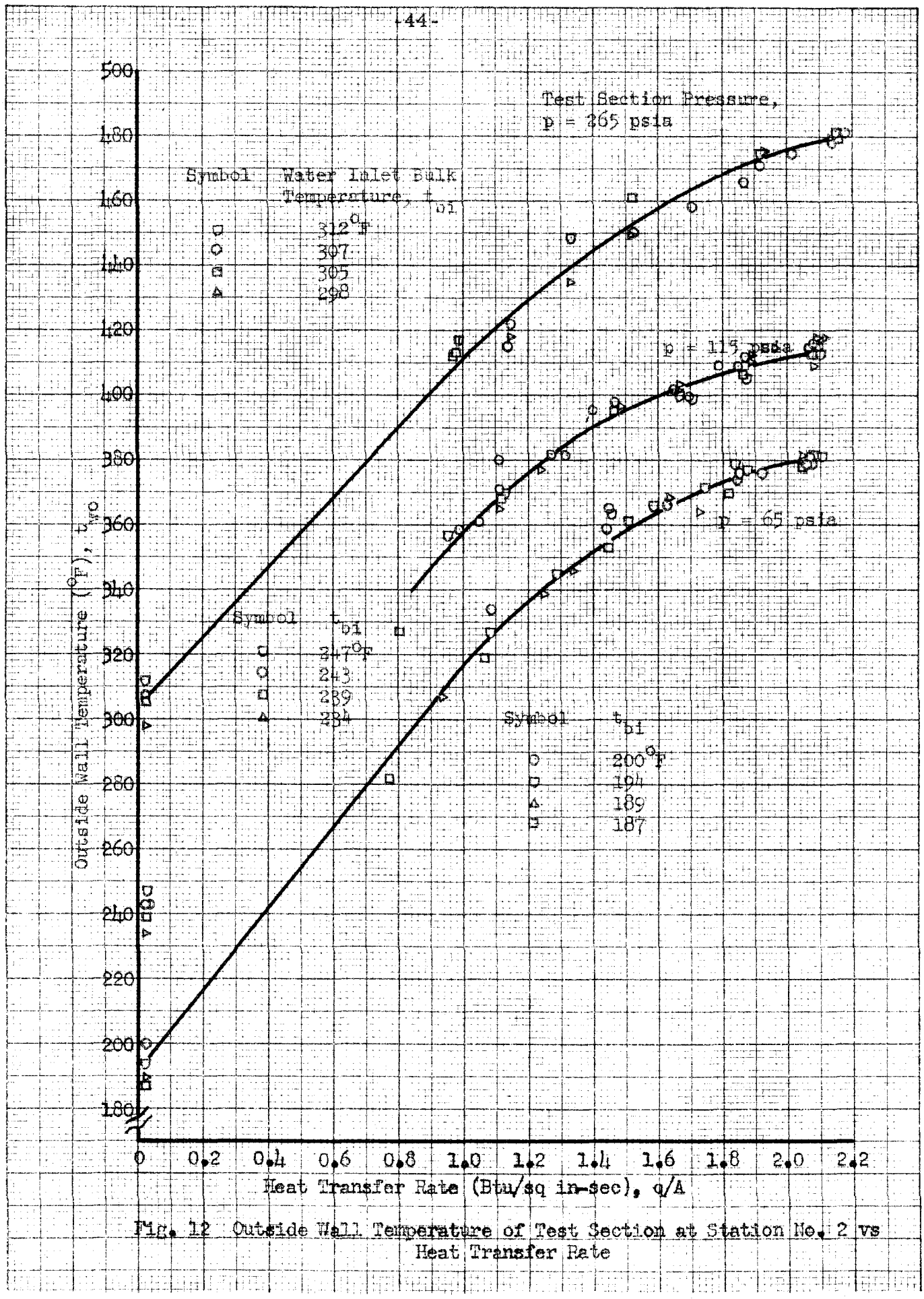

Fig. 12 Outside Wall Temperature of Test Section at Station No. 2 vs Heat Transfer Rate

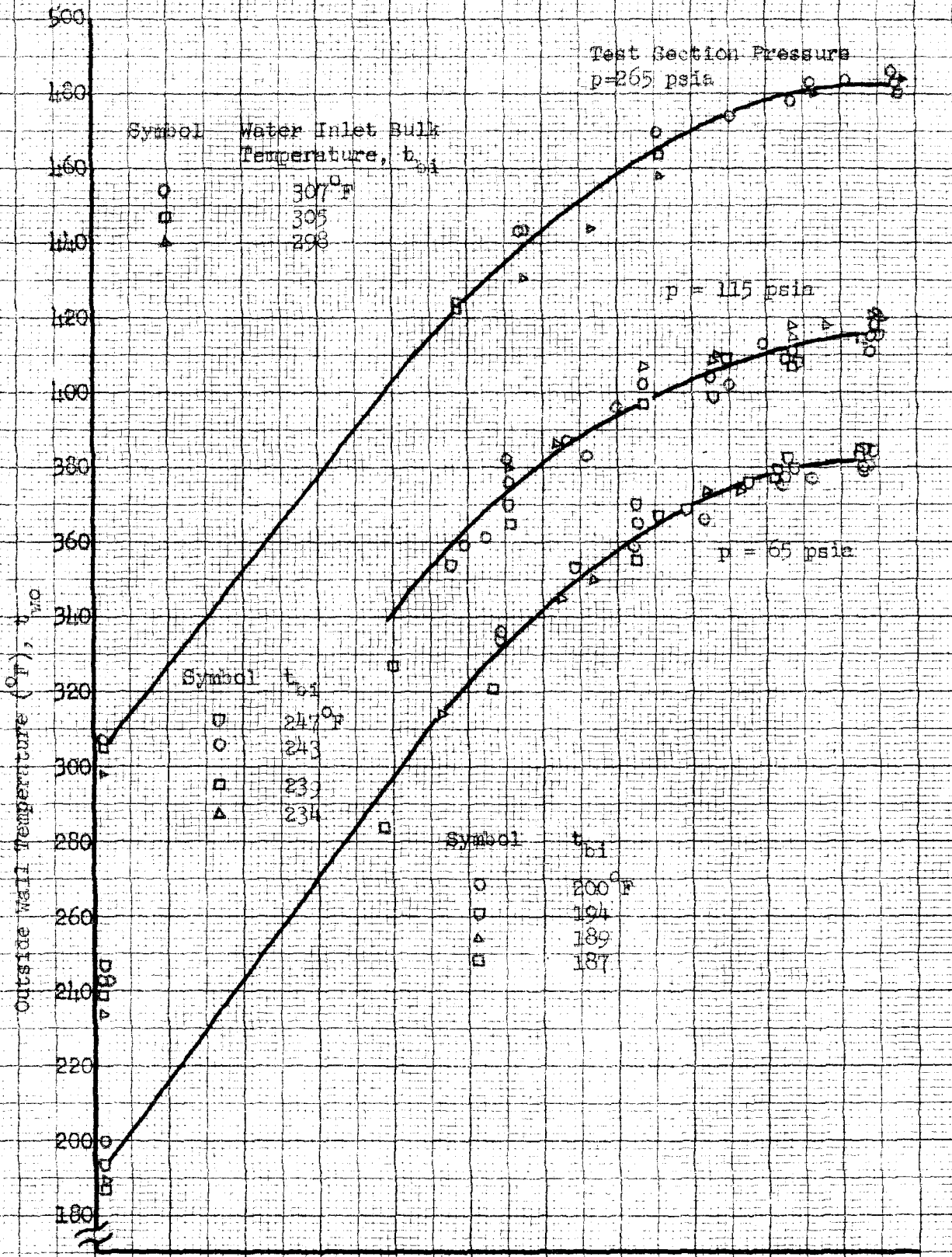

Fig. 13 Outside Wall Temperature of Test Section at Station No. 3 vs Heat Transfer Rate

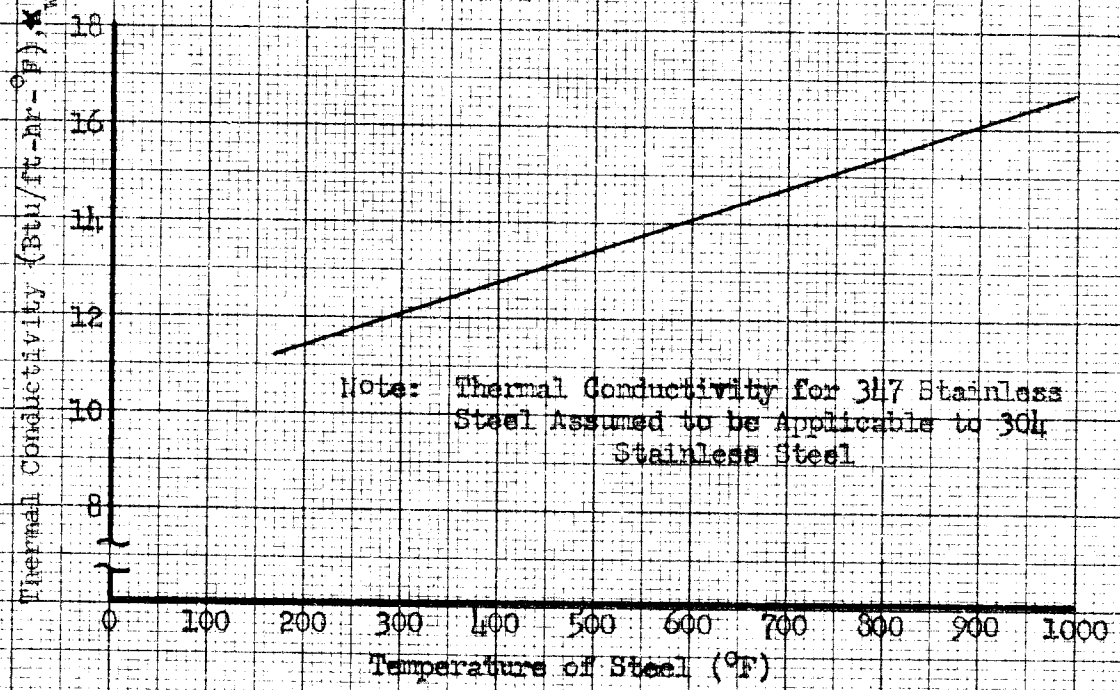

Fig. 14 Thermal Conductivity of 347 Stainless Steel vs Temperature (7)

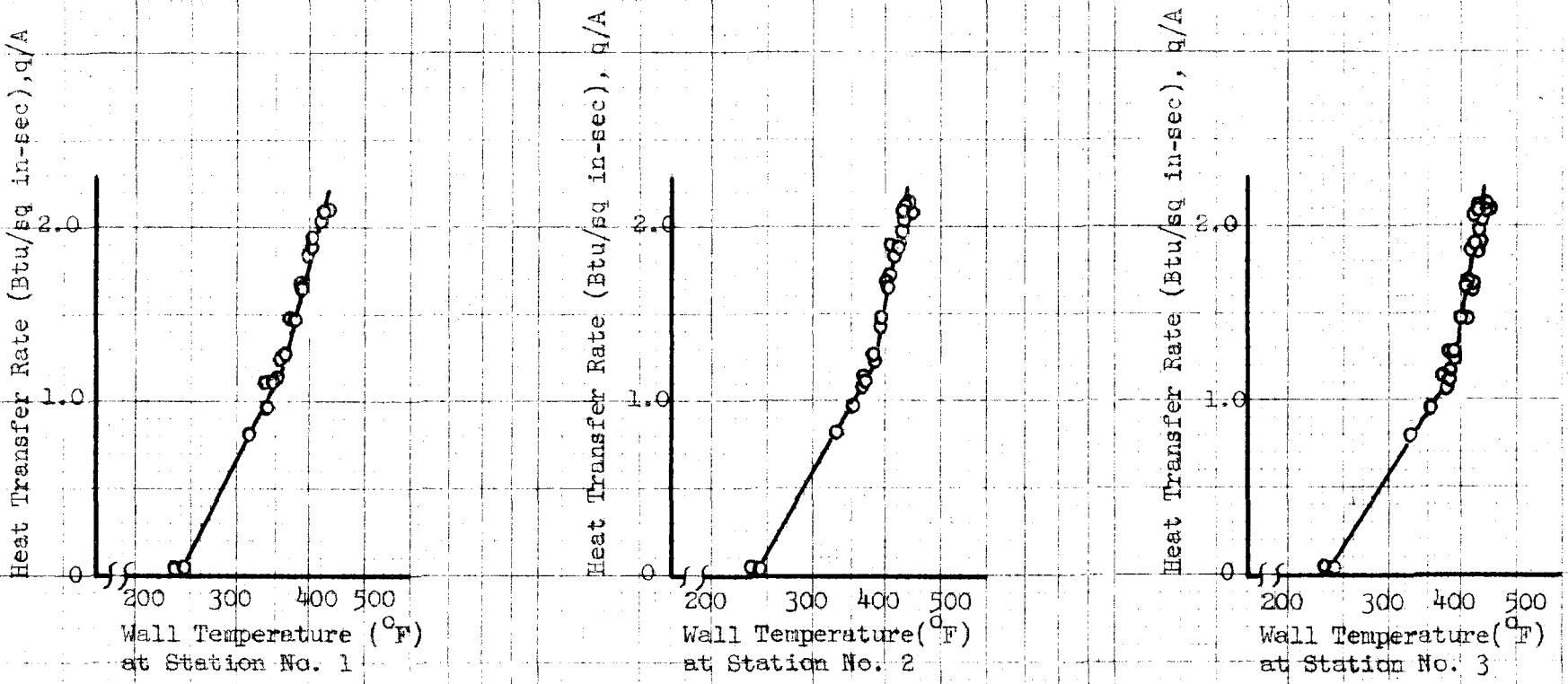

Fig. 15 Heat Transfer Rate vs Outside Wall Temperature of Test Section for Pressure of 115 psia

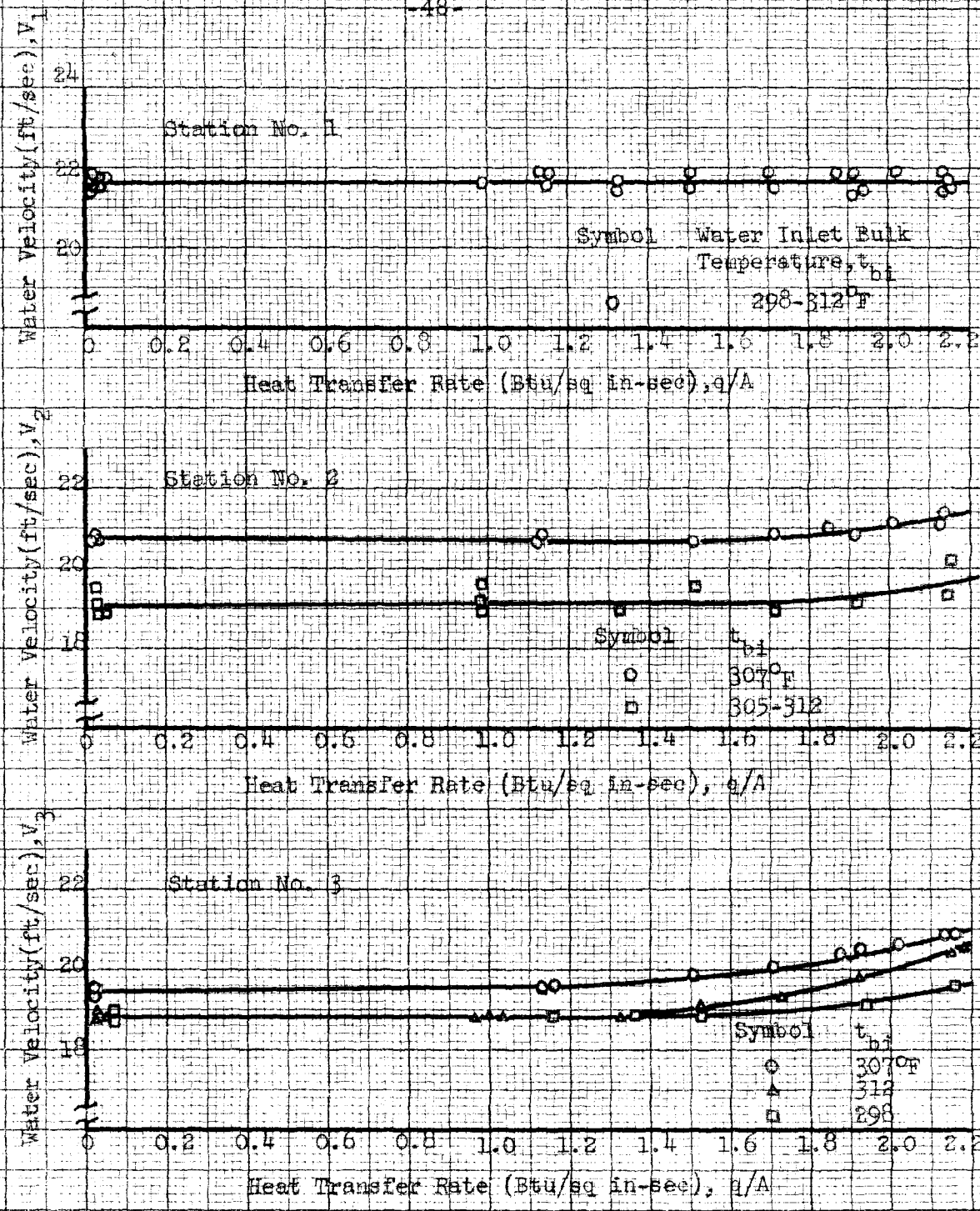

Fig. 16 Water Velocity Measurements vs Heat Transfer Rate for Test Section Pressure of 265 psia

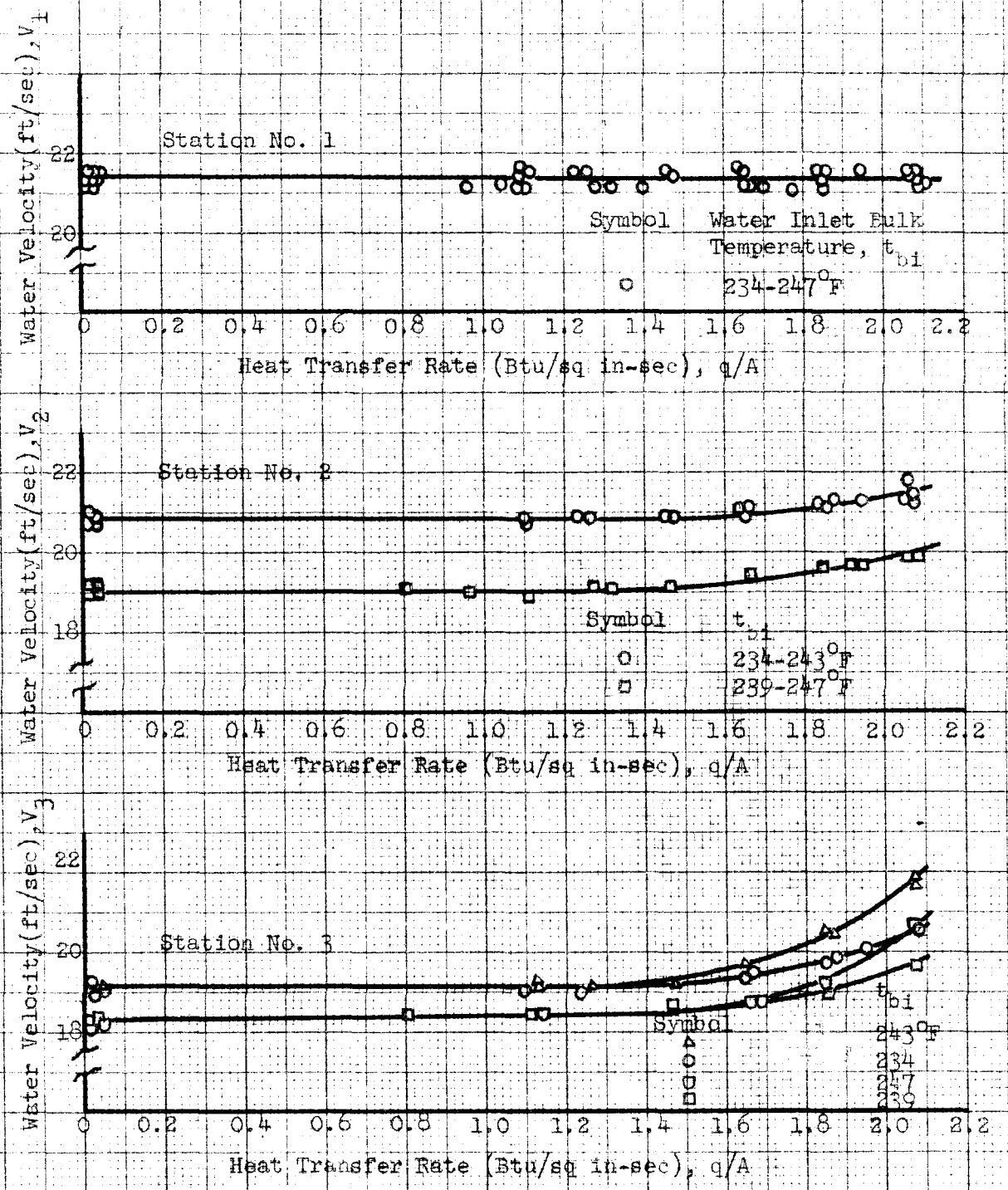

Fig. 17 Water Velocity Measurements vs Heat Transfer Rate for Test Section Pressure of 115 psia

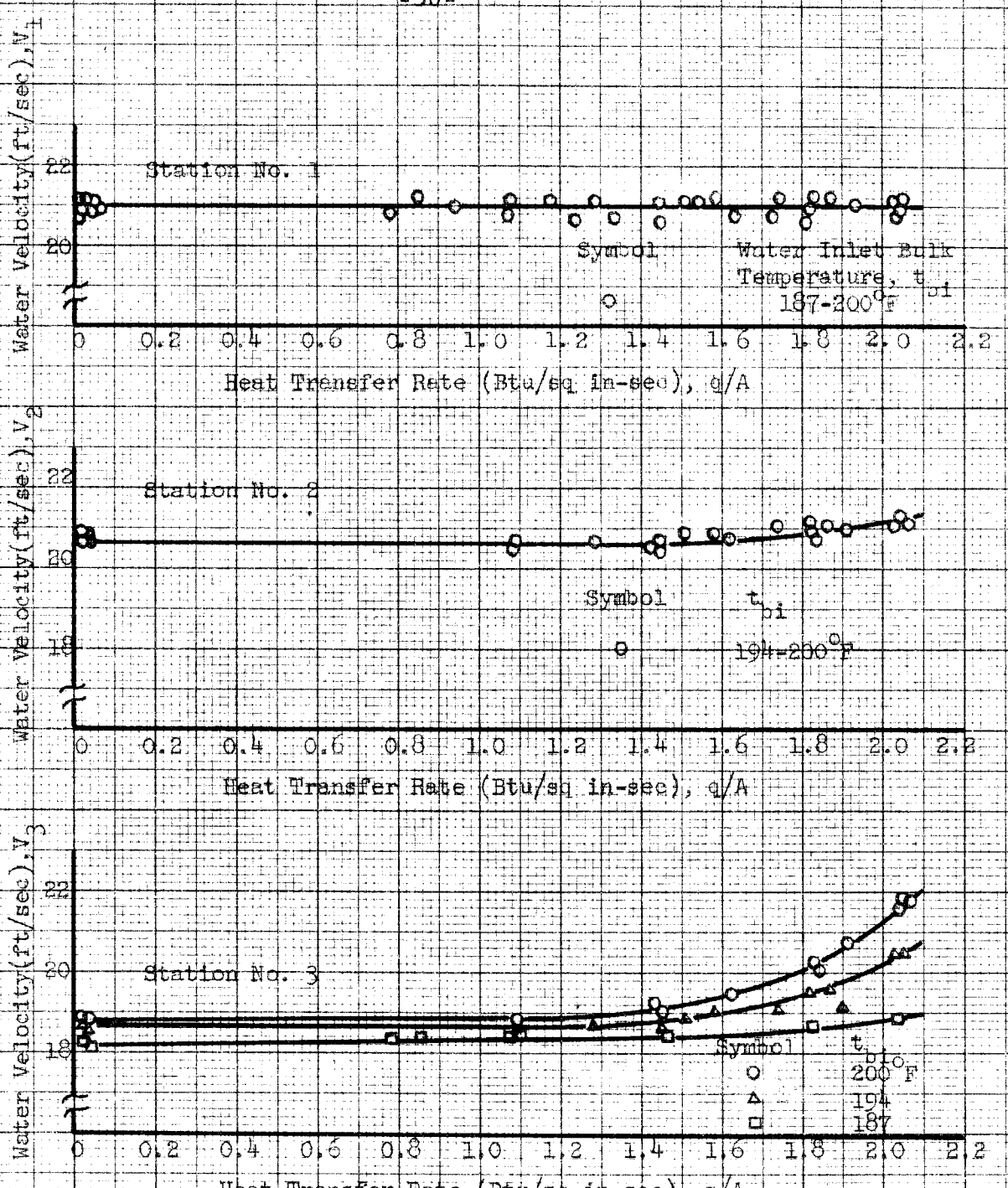

Fig. 18 Water Velocity Measurements vs Heat Transfer Rate for Test Section Pressure of 65 psia

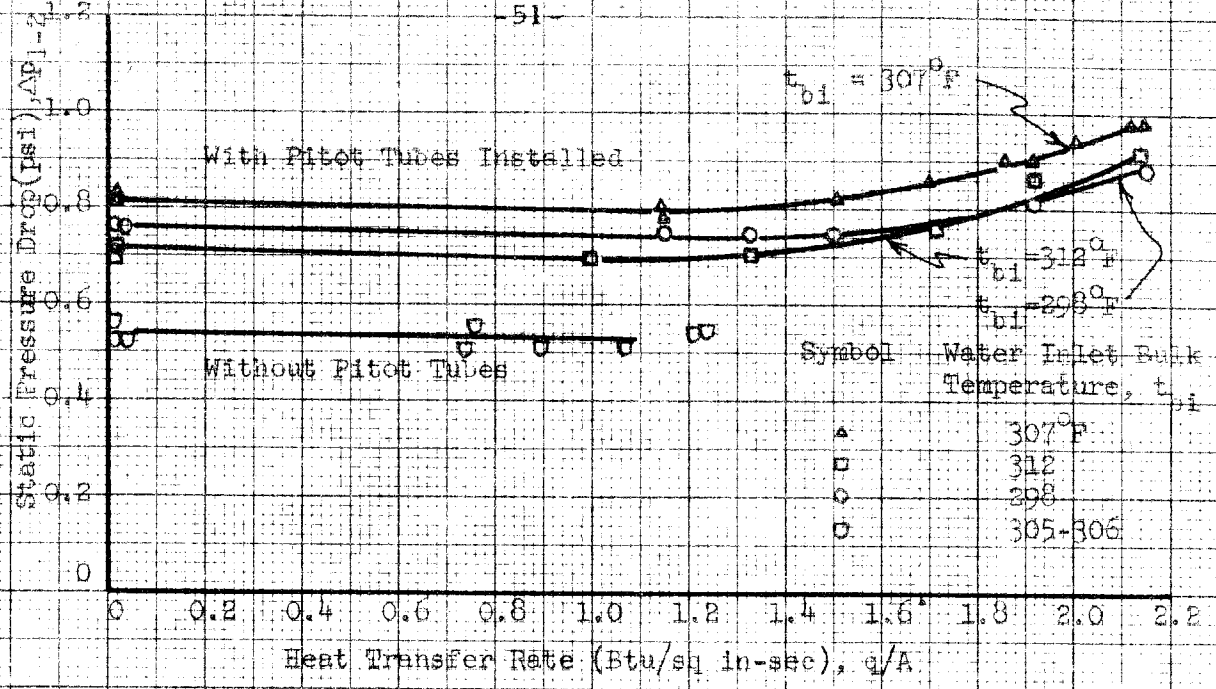

Fig. 19 Static Pressure Drop Between Stations No.1 and 2 vs Heat Transfer Rate for Test Section Pressure of 265 psia

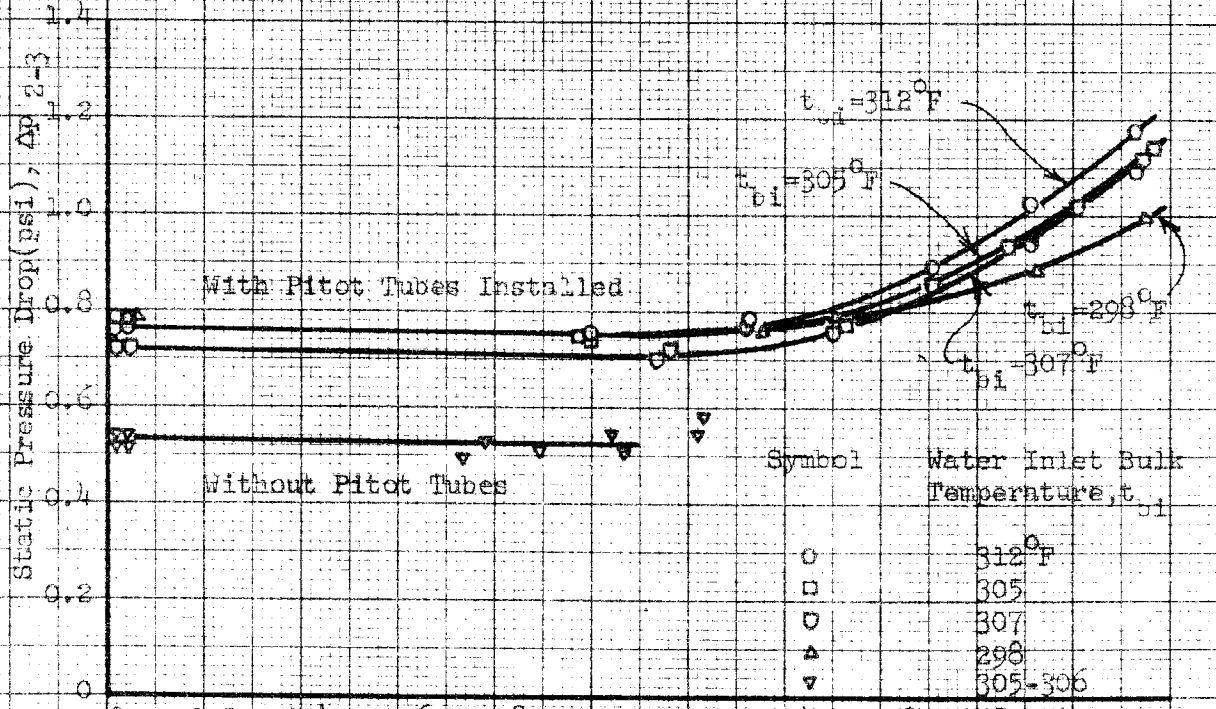

Fig. 20 Static Pressure Drop Between Stations No. 2 and 3 vs Heat Transfer Rate for Test Section Pressure of 265 psia

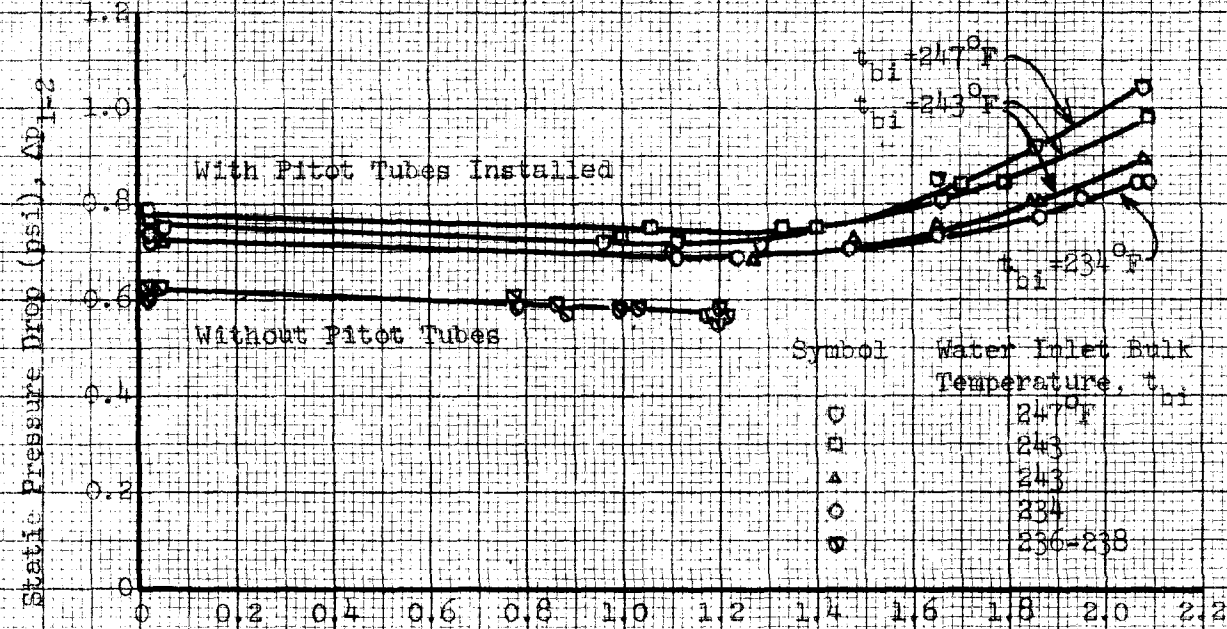

Fig. 21 Static Pressure Drop Between Stations No.1 and 2 vs Heat Transfer Rate for Test Section Pressure of 115 psia

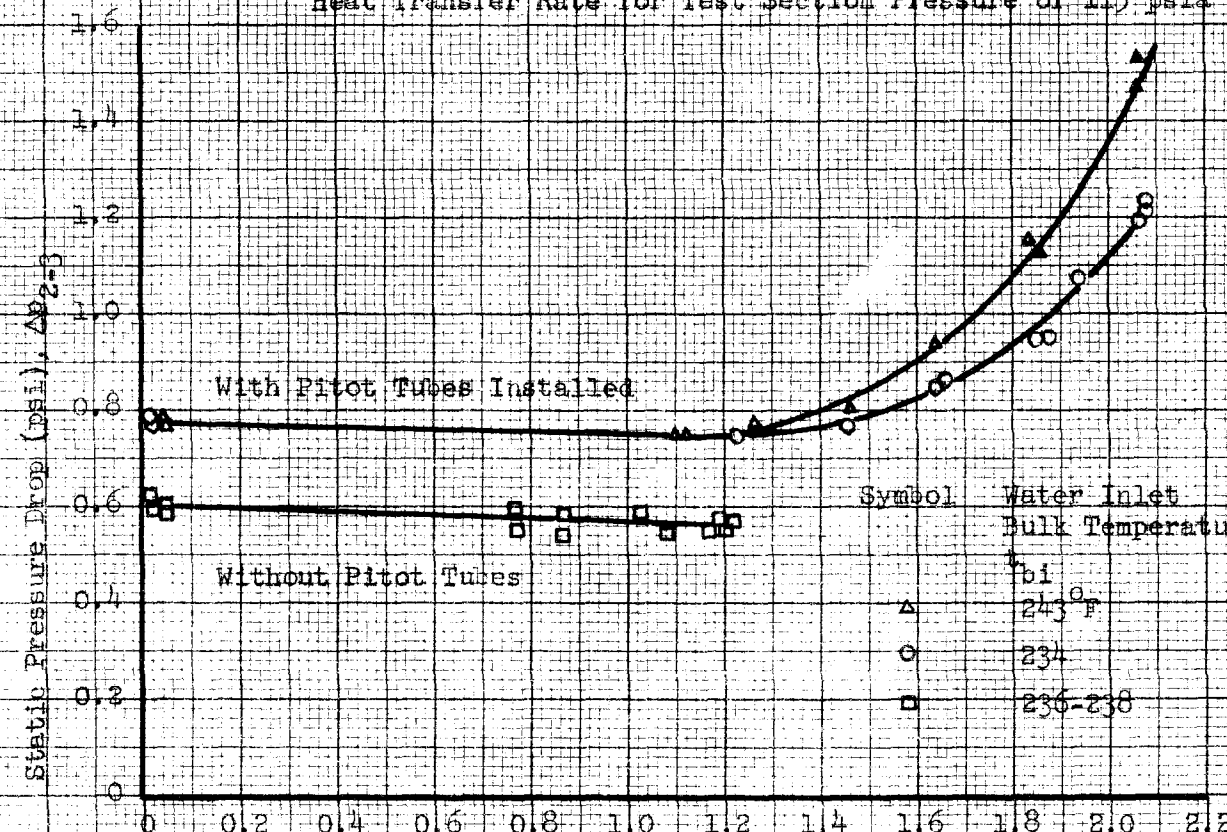

Fig. 22 Static Pressure Drop Between Stations No. 2 and 3 vs Heat Transfer Rate For Test Section Pressure of 115 psia

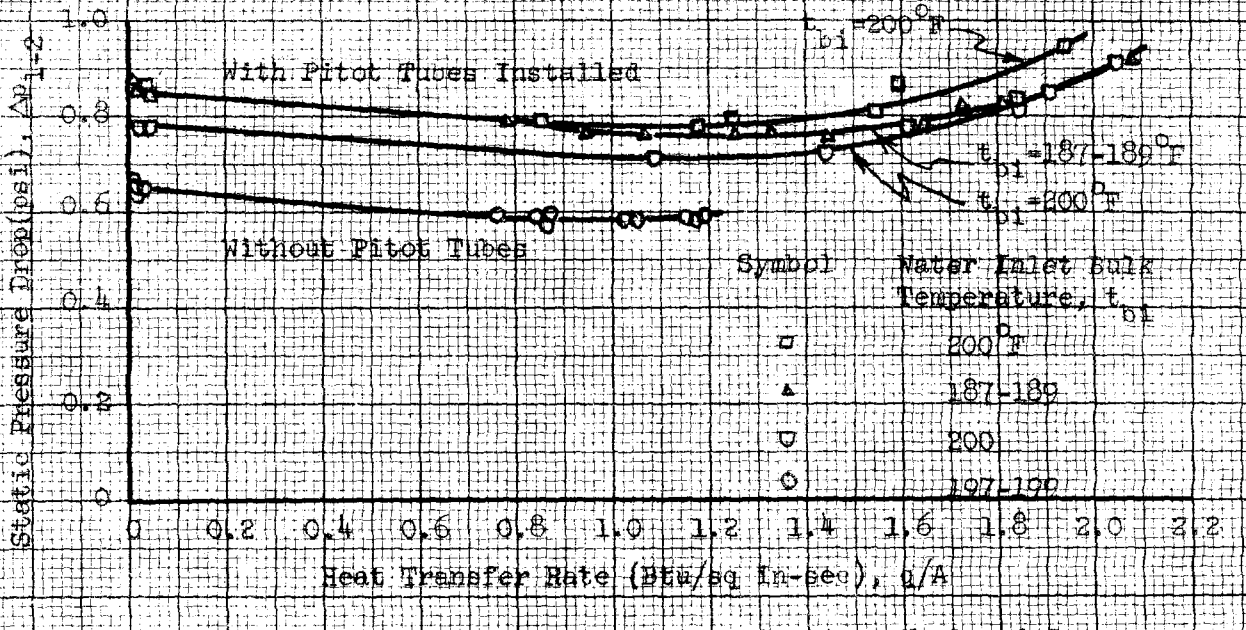

Fig. 23 Static Pressure Drop Between Stations No. 1 and 2 vs Heat Transfer Rate for Test Section Pressure of 65 psia

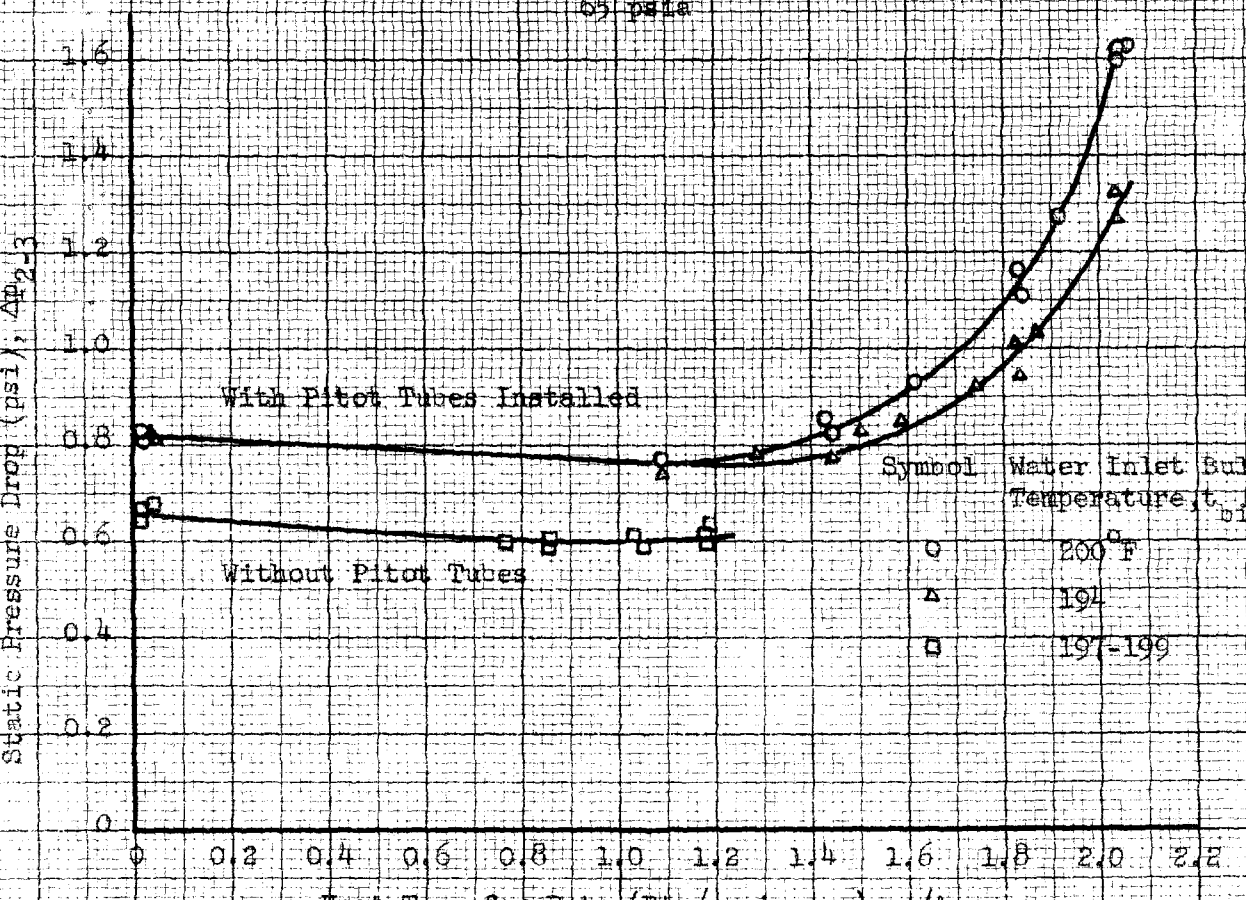

Fig. 24 Static Pressure Drop Between Stations No. 2 and 3 vs Heat Transfer Rate for Test Section Pressure of 65 psia

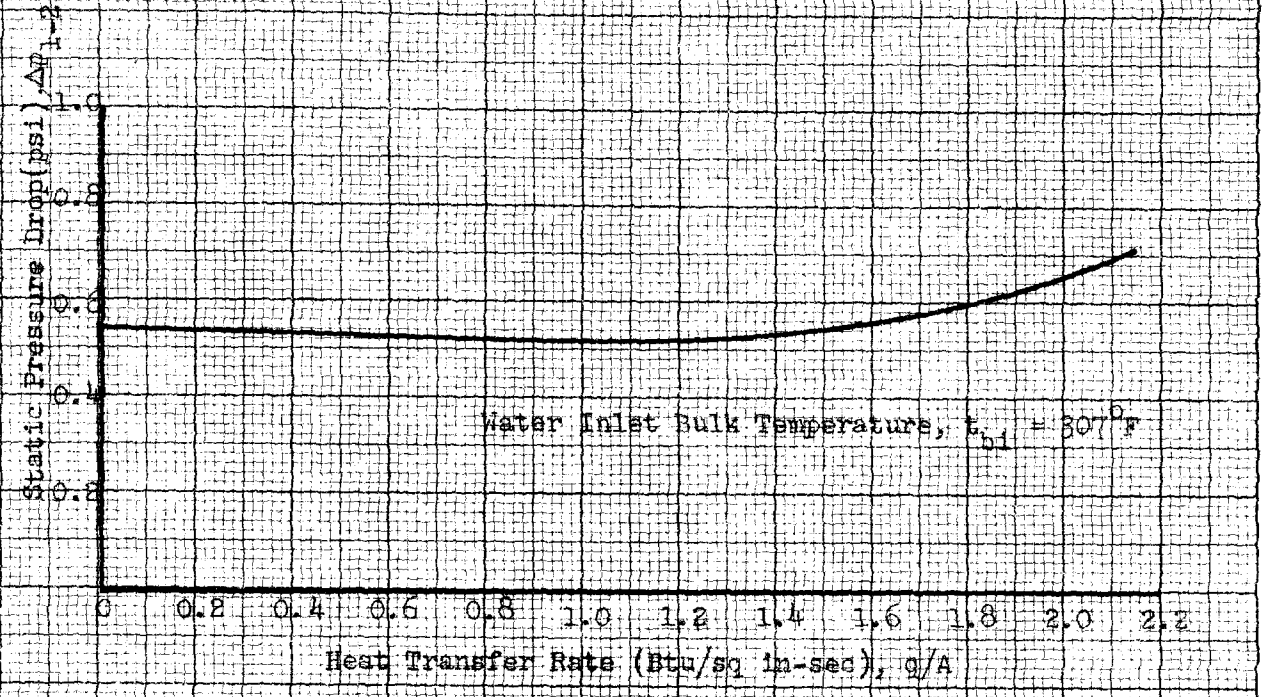

Fig. 25 Static Pressure Drop Corrected for Pitot Tube Loss between Stations No. 1 and 2 vs Heat Transfer Rate for Test Section Pressure of 265 psia

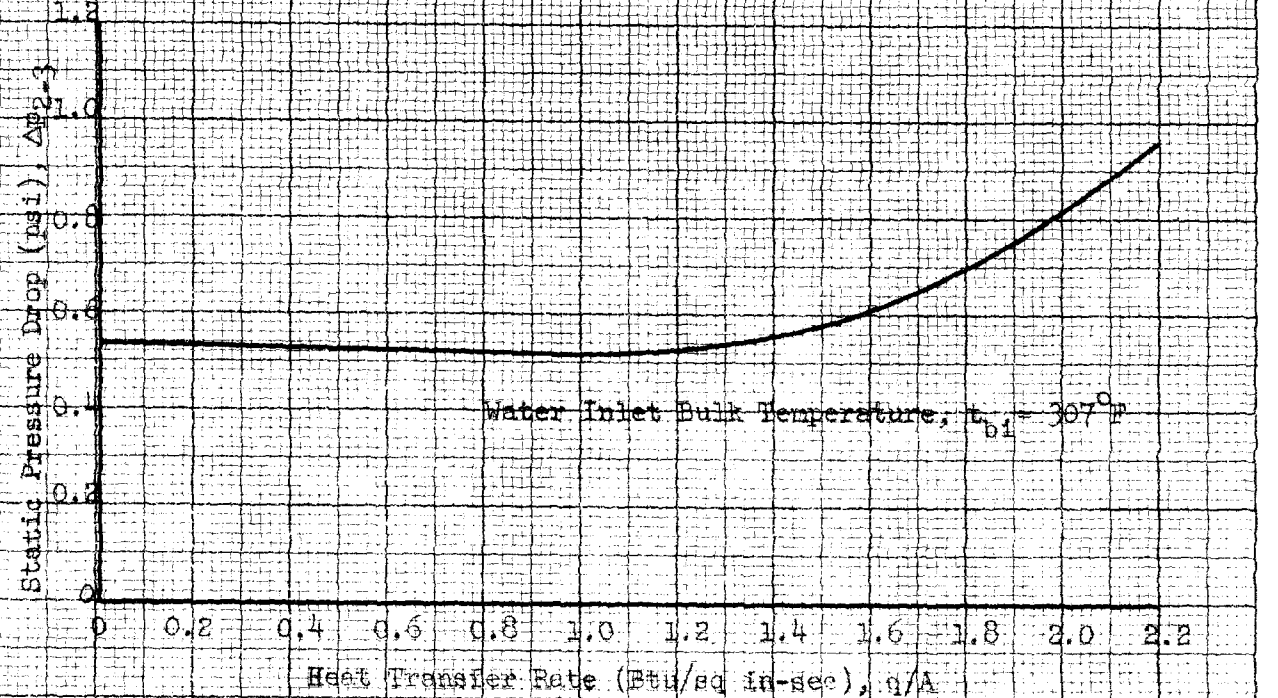

Fig. 26 Static Pressure Drop Corrected for Pitot Tube Loss between Stations No. 2 and 3 vs Heat Transfer Rate for Test Section Pressure of 265 psia

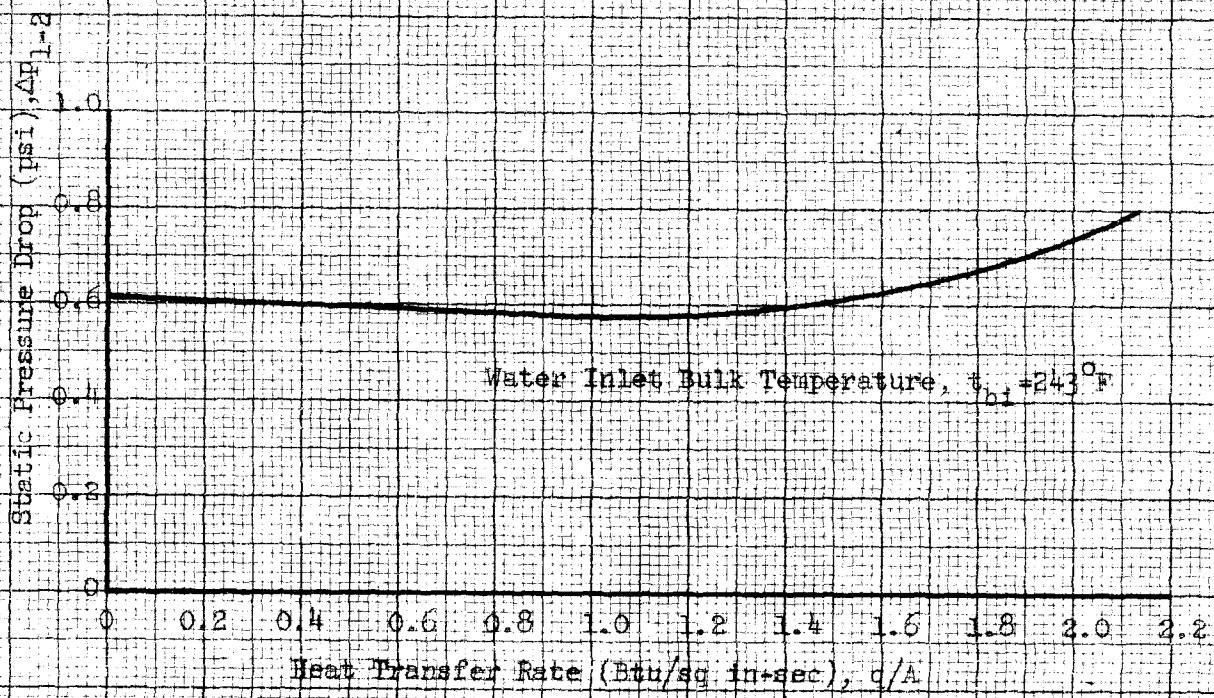

Fig. 27 Static Pressure Drop Corrected for Pitot Tube Loss between Stations No. 1 and 2 vs Heat Transfer Rate for Test Section Pressure of 115 psia

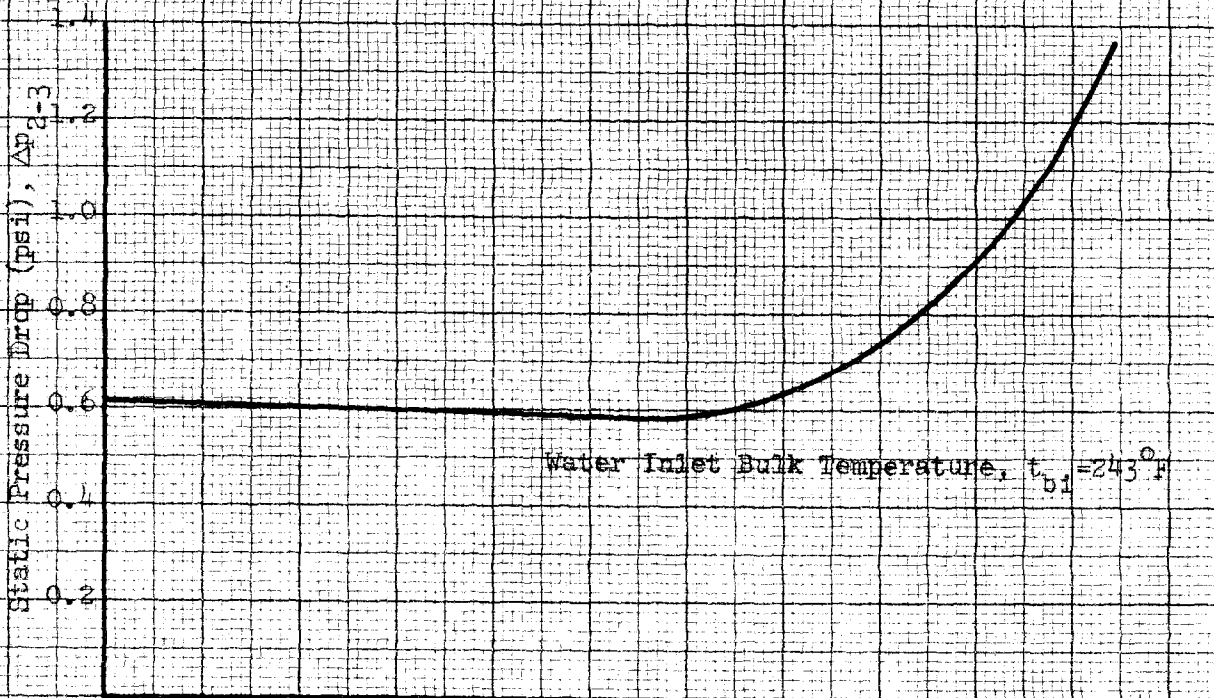

Fig. 28 Static Pressure Drop Corrected for Pitot Tube Loss between Stations No. 2 and 3 vs Heat Transfer Rate for Test Section Pressure of 115 psia

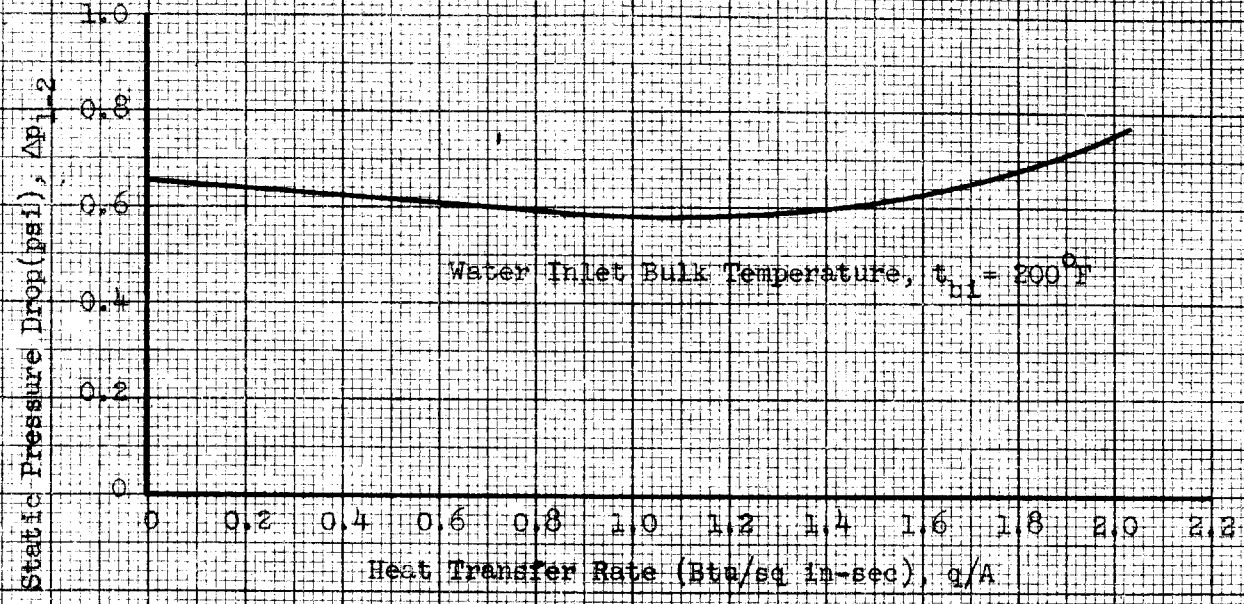

Fig. 29 Static Pressure Drop Corrected for Pitot Tube Loss Between Stations No. 1 and 2 vs Heat Transfer Rate for Test Station Pressure of 65 psia

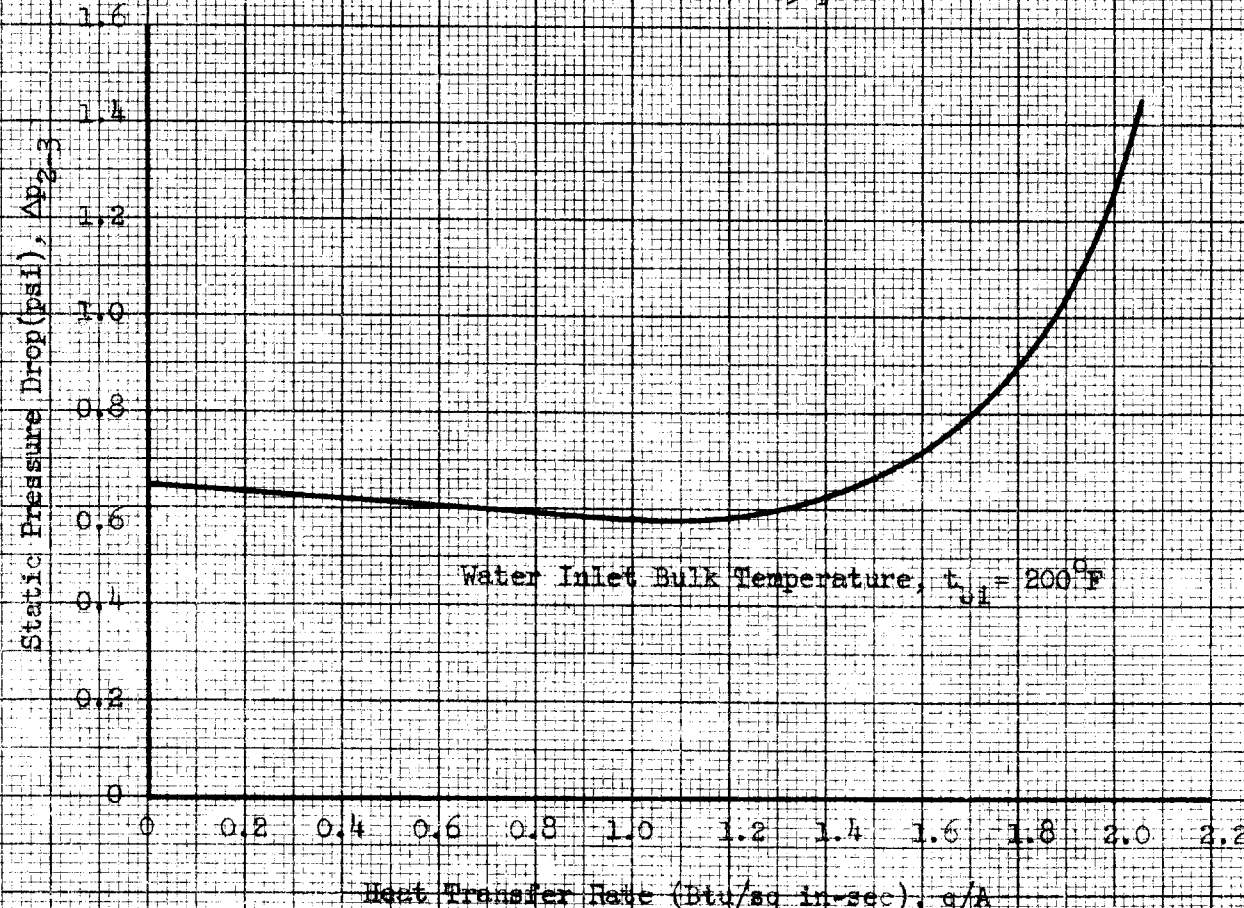

Fig. 30 Static Pressure Drop Corrected for Pitot Tube Loss Between Stations No. 2 and 3 vs Heat Transfer Rate for Test Section Pressure of 65 psia

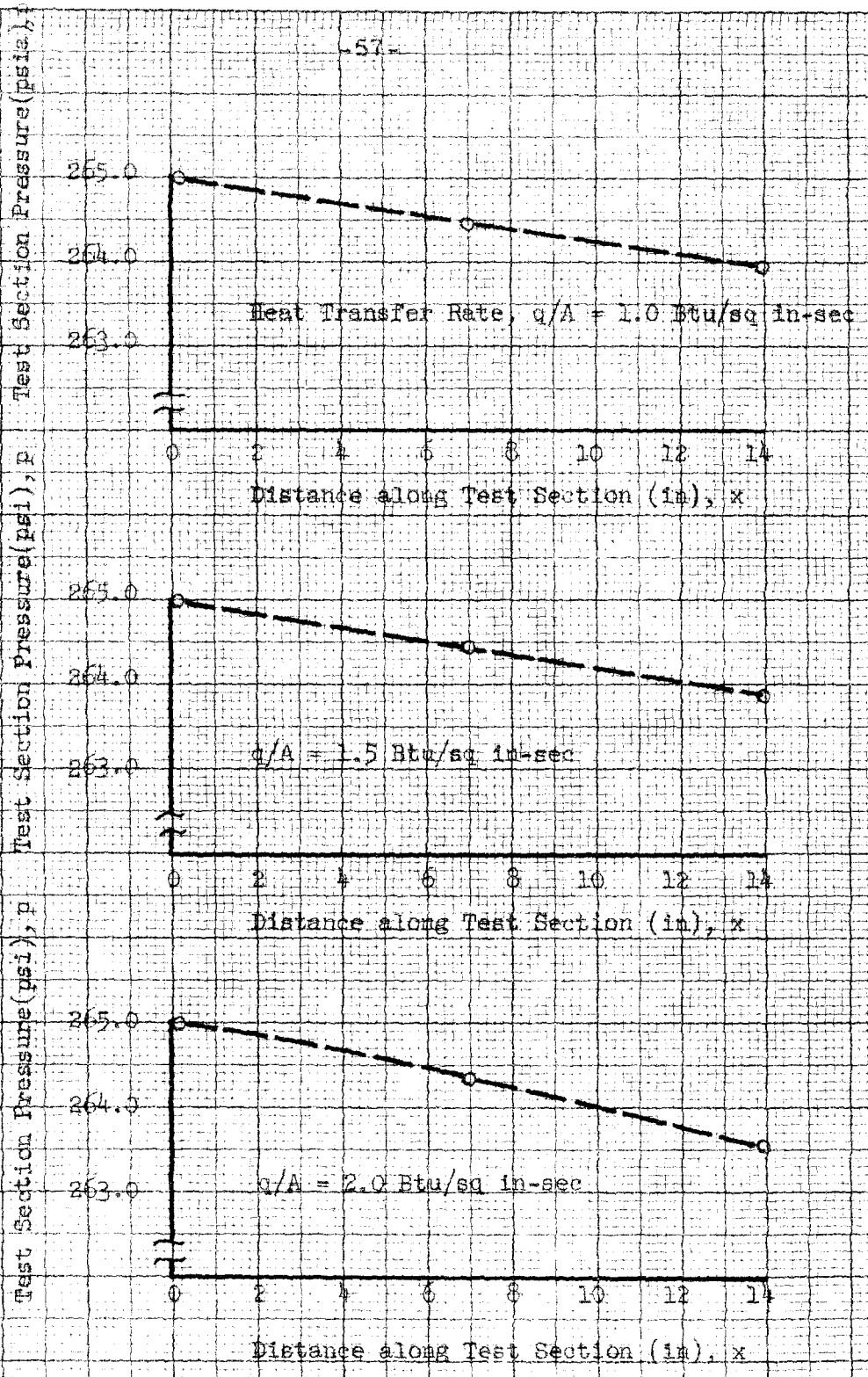

Fig. 31 Pressure Distribution along Test Section Corrected for Pitot Tube Loss for Water Inlet Bulk Temperature of 307°F

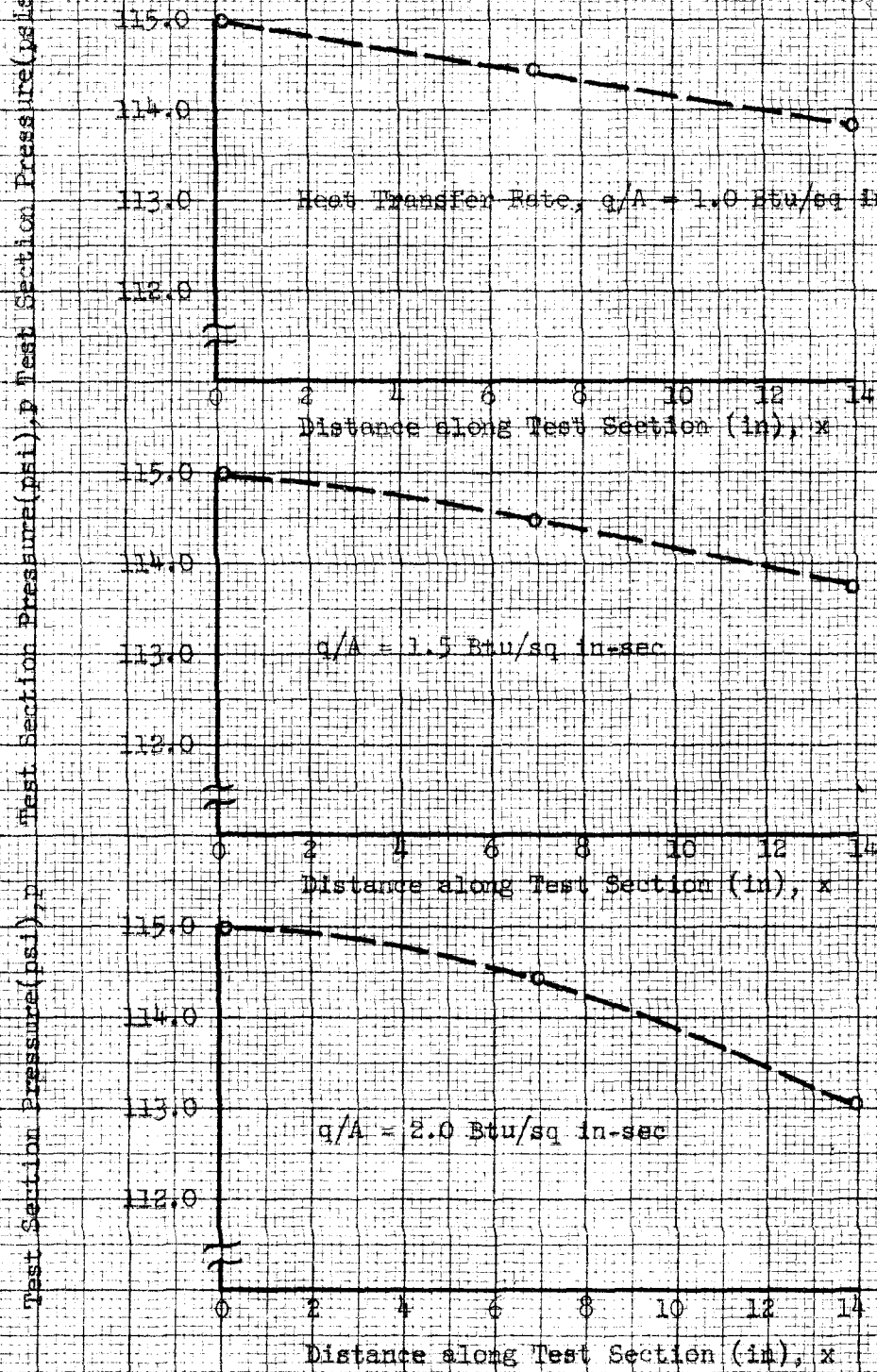

Fig. 32 Pressure Distribution along Test Section Corrected for Pitot Tube Loss for Water Inlet Bulk Temperature of 243°F

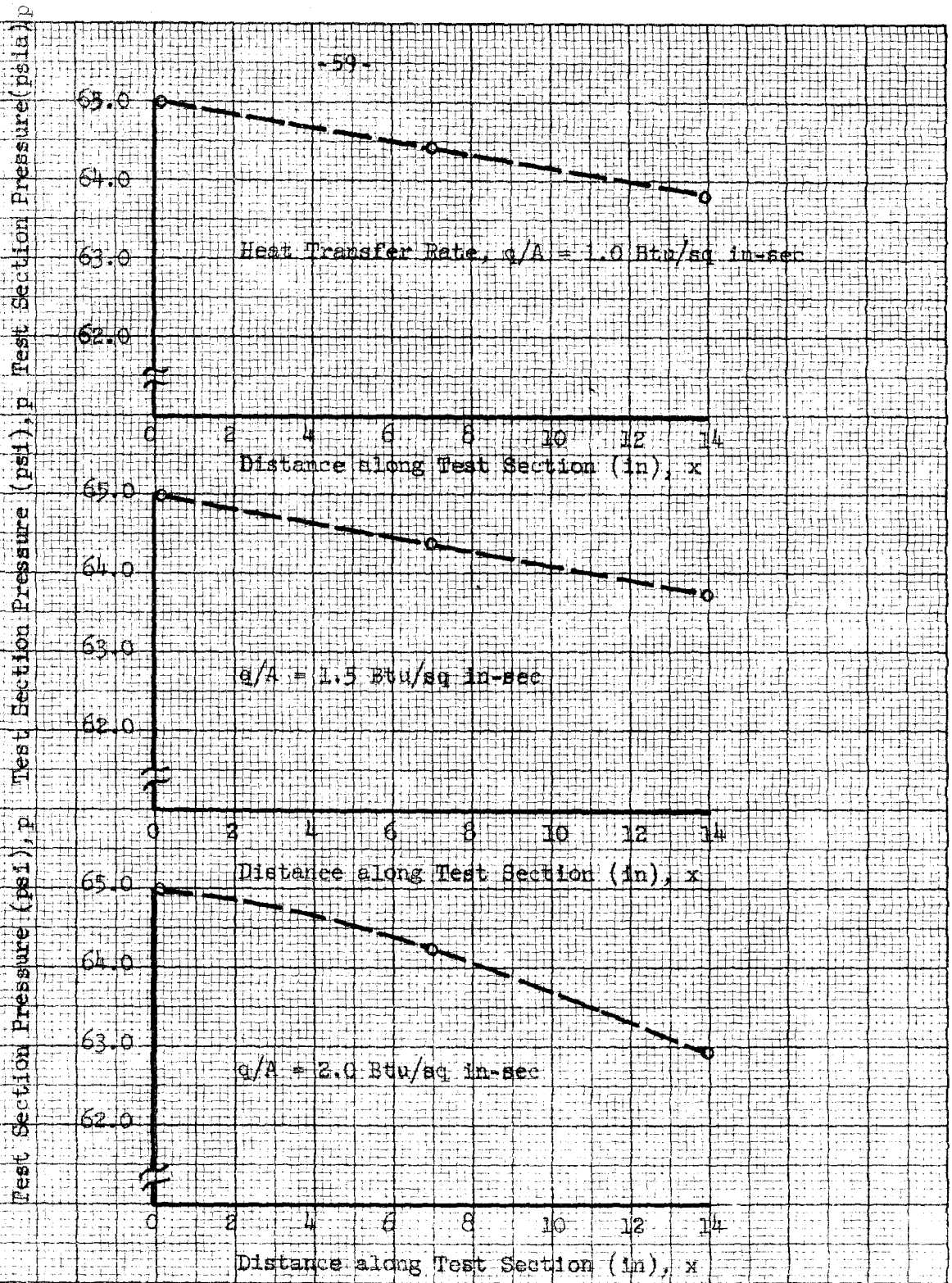

Fig. 33 Pressure Distribution along Test Section Corrected for Pitot Tube Loss for Water Inlet Bulk Temperature of 200°F

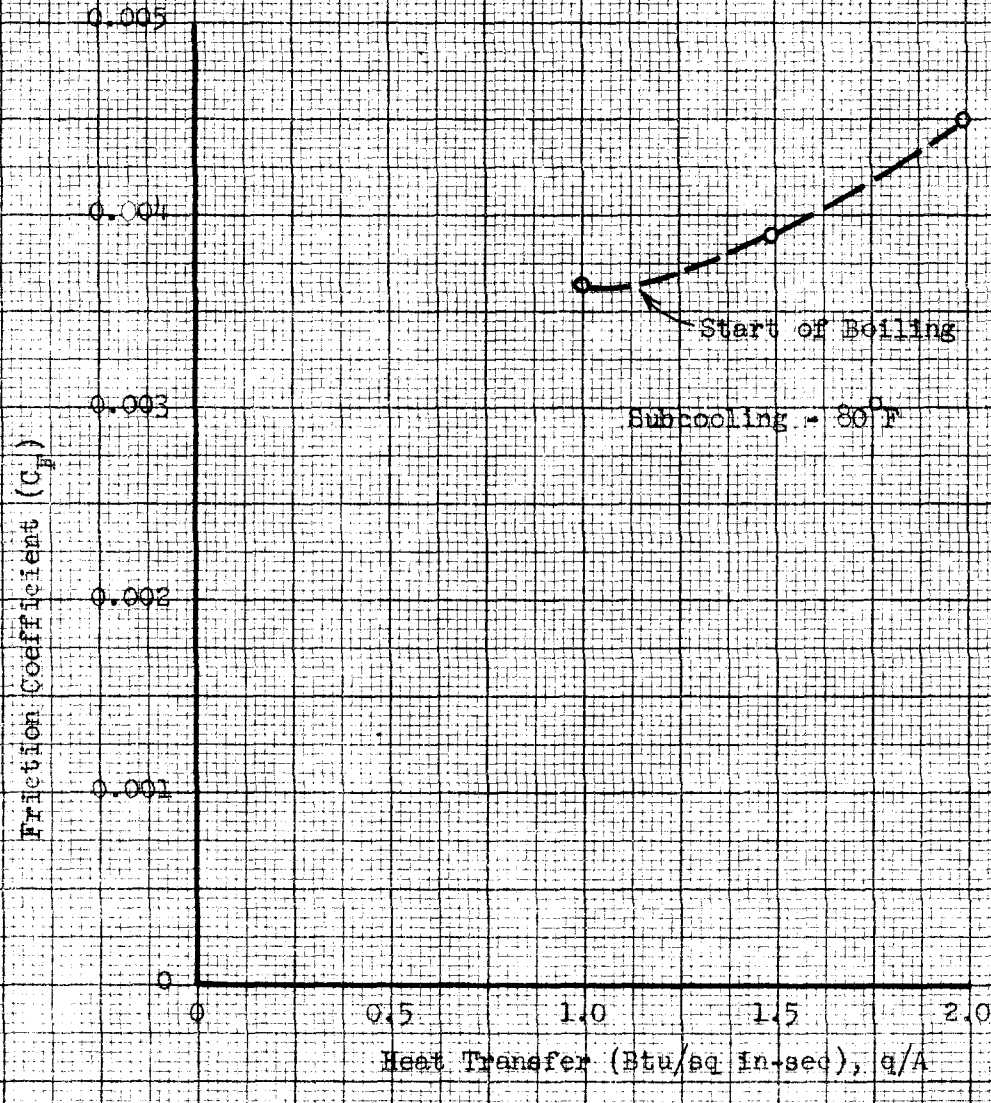

Fig. 34 Friction Coefficient vs Heat Transfer Rate for Test Section Pressure of 115 psia

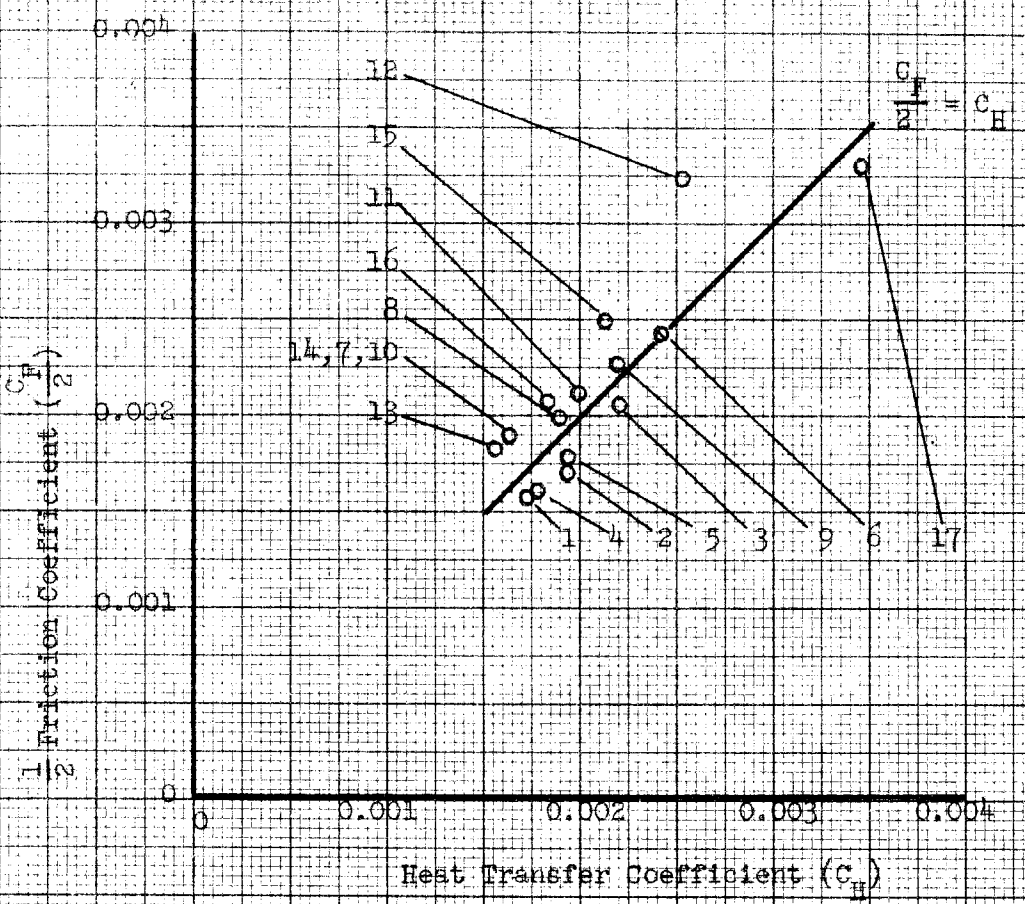

Symbol	Subcooling (t_s)	Heat Transfer q/A (Btu/sq ft-sec)	Inlet Bulk Temp. (t_M)	Pressure (psia)	Symbol	Subcooling (t_s)	Heat Transfer q/A (Btu/sq ft-sec)	Inlet Bulk Temp. (t_M)	Pressure (psia)
1	80	1.0	307	265	10	77	1.0	243	115
2	80	1.5	307	265	11	68	1.5	243	115
3	80	2.0	307	265	12	59	2.0	243	115
4	82	1.0	307	265	13	80	1.0	200	65
5	73	1.5	307	265	14	80	1.5	200	65
6	64	2.0	307	265	15	80	2.0	200	65
7	80	1.0	243	115	16	71	1.5	200	65
8	80	1.5	243	115	17	62	2.0	200	65
9	80	2.0	243	115					

Fig. 35 One-half Coefficient of Friction vs Coefficient of Heat Transfer